Shock Waves (2022) 32:517–537
https://doi.org/10.1007/s00193-022-01090-6

ORIGINAL ARTICLE

Combustion properties of a simple and efficient four-step model

M. Peswani[1] · C. Gerace[1,2] · B. Maxwell[1]

Received: 13 January 2022 / Revised: 30 May 2022 / Accepted: 27 June 2022 / Published online: 17 August 2022

Abstract
Modeling of the chemistry and thermodynamics is crucial in numerical simulations that attempt to accurately simulate reactive flows such as flame acceleration and detonation phenomena. The current study explores how a four-species, four-step combustion mechanism performs to predict ignition processes in various premixed hydrocarbon fuel mixtures when compared to detailed chemical kinetic mechanisms. A key objective of this research is to determine how well this model, which has been modified to include only three species transport equations, performs at predicting fundamental combustion properties that are important for flame acceleration and detonation applications. On comparison with full chemistry mechanisms, the four-step model demonstrates an ability to predict the ignition time, reaction stiffness, thermodynamic state, and detonation stability-parameter to a high level of accuracy, for ignition processes over a wide range of initial temperatures and densities. With the ignition structures and key detonation stability parameters correctly predicted, we conclude that the four-step model is an effective and economic tool for studying complex explosion phenomena in situations where pre-combustion temperature and density are constantly changing, such as deflagration-to-detonation transition by flame acceleration or shock–flame interaction.

Keywords Detonations · Premixed combustion · Combustion properties · Global reaction mechanism

1 Introduction

Reactive flows generated by shocks, such as detonation waves, are highly compressible in nature with experimental results available only for highly idealized and controlled cases. Such experiments are often conducted with limited quantitative and temporally evolved diagnostics, owing to the high-speed nature of the wave. For complex phenomenon such as deflagration-to-detonation transition (DDT), even basic sufficient requirements for transition to occur are unknown, with experimental results being highly stochastic [1]. These difficulties make such flows prime candidates for investigation using numerical methods, in order to obtain better quantitative and qualitative descriptions of the flow. Gaseous detonations are supersonic self-sustained combustion waves that consist of a strong leading shock coupled to a trailing reaction zone. Following early investigations into transient detonation phenomenon [2,3], it became evident that numerical simulations must require realistic characterization of the chemical properties of the gas mixtures involved with results from simplified combustion models leading to incorrect basic results [4,5]. The current study assesses the performance of a reduced four-step combustion model based on a thermochemical approach for a range of premixed hydrocarbon mixtures, to better characterize the thermodynamic behavior of such flows and provide better chemical response closure in numerical simulations.

Chemical kinetic models in all combustion applications can be classified into two main categories: (1) elementary reaction mechanisms (ERMs) and (2) global reaction mechanisms (GRMs). Elementary reaction mechanisms provide the most precise description of reactive flows through single-transition-state reactions among real chemical species, while

Communicated by G. Ciccarelli.

✉ M. Peswani
mohnish.peswani@case.edu

C. Gerace
22gerchr@hawken.edu

B. Maxwell
brian.maxwell@case.edu

[1] Department of Mechanical and Aerospace Engineering, Case Western Reserve University, Euclid Ave 10900, Cleveland, OH 44106, USA

[2] Hawken School, County Line Rd 12465, Gates Mills, OH 44040, USA

GRMs are formulated to cover only the dominant reaction paths through simplified global reactions steps. In order to provide an accurate description of the chemistry, ERMs typically include numerous chemical species and reaction steps that limit their application for full-scale multi-dimensional numerical simulations because of the large computational cost and memory requirements. Through the elimination of species that are redundant (skeletal ERMs) [6–9], followed by time-scale analysis and removal of quasi-steady-state (QSS) species [10–12], it is possible to create a moderate-sized ERM that is still precise within a specific scope. However, the extent to which the mechanism can be reduced using these approaches is limited [13] and has only been successfully realized for a few reactive hydrocarbon mixtures such as those involving methane [7], acetylene [10], and ethylene [14]. It was also observed that for hydrocarbons, the minimum number of species for a reduced skeletal ERM reaches a value of around 10, after which further simplification is not feasible [15].

To date, a vast majority of numerical detonation research has instead applied idealized GRMs, the most common one being the standard one-step Arrhenius reaction model [16]. While the one-step model has been crucial for theory development as well as for investigating the influence of the global activation energy and heat release on detonation propagation [17], it has several severe limitations. In a typical reaction, the temporal structure consists of a relatively long and nearly thermally neutral induction time followed by a comparatively short exothermic reaction time, in which the majority of the heat is released. In the simple one-step model, however, there is no explicit thermally neutral induction phase. Heat is always released, and there is no independent control of the induction/reaction zone scales. As a result, the model cannot accurately reproduce the temporal reaction structures and stiffness associated with combustion. For detonation waves, the single global activation energy in the one-step model also controls both the spatial structures of the induction and reaction zones simultaneously and therefore cannot reproduce the correct steady Zel'dovich–von Neumann–Doring (ZND) structure in a detonation wave [18]. In fact, the ratio of the induction to reaction zone lengths has been shown to be an important parameter that controls the multidimensional cellular stability of detonation waves [19].

An extension to this one-step model is a two-step model [20,21], which consists of a strictly thermally neutral induction stage followed by a state-insensitive exothermic stage. However, the model assumes that the chain branching explosion is instantaneous, with the fuel converted to radicals once the induction time is reached. This is inaccurate for reactive mixtures involving acetylene or hydrogen, where chain branching cross-over temperature effects influence ignition delay time response to changes in temperature, and consequently the detonation structure [22,23]. To account for such changes in gas sensitivity to temperature, a three-step model has also been developed and investigated in great detail [22,24,25]. The model has the advantage of being able to handle chain-branching crossover effects, but still lacks the independent control of length and time scales in each of the induction and reaction zones. Detonation problems, however, are highly stiff with a wide range of length and time scales that must be resolved and captured. Here, stiffness is defined as a property of a differential equation where the rates of change of a measured quantity are significant. To capture the correct stiffness, through independent control of the different reaction zones, is therefore of significant importance to accurately predict the rapidly changing thermodynamics that govern the physics of flame acceleration or detonation phenomenon. Four-step models [26] with an added chain-termination step and five-step models [27] which account for radical competition have also been proposed in the past but are mainly limited to hydrogen combustion. Typical applications of these idealized GRMs also assume the reactive mixture to be a calorically perfect gas (i.e., heat capacities remain constant) leading to incorrect post-shock and post-combustion states. As a result, such perfect gas assumptions may not respond appropriately for situations where initial states are constantly changing, such as DDT arising from flame acceleration [28,29], or shock–flame interaction scenarios [30].

In order to address the shortcomings of the models described above, a simple four-species, four-step reaction mechanism based on a thermochemical approach was proposed by Zhu et al. [31] for premixed reactive hydrocarbon mixtures. This combustion model is a GRM that utilizes discrete packs of chemical species as global species which mimic the behavior of a detailed chemistry ERM. By assuming the gas mixture to be thermally perfect, i.e., ideal gas behavior with temperature-dependent heat capacities, the model is able to respond appropriately to changes in the thermodynamic state. Through independent calibration of the reaction rate constants throughout the combustion regime, the model has been previously demonstrated to capture the detailed chemistry ignition temperature evolution for constant volume and constant pressure ignition problems for stoichiometric acetylene–oxygen combustion [31]. Since detonation waves involve the coupling of gas dynamics and chemical reactions, and influenced by changes in the thermodynamic properties of the medium, the model was also demonstrated to correctly predict the one-dimensional ZND

reaction structure in stoichiometric acetylene–oxygen to a high level of accuracy.

In this work, an in-depth analysis of the four-step model is carried out for several premixed reactive hydrocarbon mixtures with very different activation energies, ignition characteristics, and detonation stability. In particular, we highlight the model's ability to predict important properties required for simulating realistic scenarios involving flame acceleration and detonations. The main properties of interest are the ignition delay, Chapman–Jouguet (CJ) velocity, expansion ratio, Zel'dovich number, activation energy, heat release, and detonation χ parameter for a wide range of conditions. In addition to stoichiometric fuel–oxygen mixtures, the four-step model performance has also been assessed for cases of heavy dilution as well as fuel lean ($\phi < 1.0$) mixtures. Finally, following the results and discussions presented in Sects. 3 and 4, a summary of the limitations of the four-step model with regard to simulating combustion of fuel-rich mixtures and reactive hydrogen mixtures is covered. In this sense, we aim to determine the applicability and restrictions of the four-step, four-species model to be used as an effective reduced GRM for accurately modeling flame acceleration, supersonic combustion, and detonation waves in a variety of reactive hydrocarbon mixtures.

2 Four-step combustion model methodology and calibration

The global species in the four-step model are calibrated from the equilibrium results for a premixed combustion system using Cantera's [32] built-in minimum Helmholtz energy equilibrate function. The compact global species system for a generic fuel C_xH_y has been summarized by Zhu et al. [31] as

$$\begin{cases} C_xH_y + (x + y/4 + z) \cdot O_2 & \rightarrow R \\ \rightarrow x \cdot CO_2 + (y/2 \cdot H_2O + z \cdot O_2) & \rightarrow P1 \\ \rightleftharpoons x \cdot CO + y \cdot H + (x + y/2 + 2z) \cdot O & \rightarrow P2, \end{cases} \tag{1}$$

with $z \geq 0$ ($z = 0$: stoichiometric; $z > 0$: lean). The global species adequately predict the initial and terminal states of a combustion process, but not the intermediate stages. The reaction paths are then built by fitting the reference data from a constant volume process for an ERM of choice using Cantera [32]. This is done by substituting the global species for a reactive mixture (R, P1, and P2) into the process while conserving the overall thermodynamic properties. The reaction paths, and corresponding reaction rates and orders, are acquired by modeling the reaction as having two thermally neutral induction regime paths, two irreversible exothermic reaction paths that convert R to P1 and P2 separately, and an additional equilibrium step between P1 and P2.

The reaction scheme can be summarized as

$$\begin{cases} \text{(i1)} & R0 \rightarrow R1 & k_{i1} \\ \text{(i2)} & R0 + s_0 \cdot R1 \rightarrow (1 + s_0) \cdot R1 & k_{i2} \\ \text{(r1)} & R1 \rightarrow \delta_1 \cdot P1 & k_{r1} \\ \text{(r2)} & R1 \rightarrow \delta_2 \cdot P2 & k_{r2} \\ \text{(e)} & P1 \rightleftharpoons \delta_3 P2 & k_{ef}, k_{er}, \end{cases} \tag{2}$$

where the absolute rate constants k_i, k_{r1}, k_{r2}, k_{ef}, and k_{er} rely only on the local thermal state of the mixture, while the stoichiometry coefficients are: $\delta_1 = W_R/W_{P1}$, $\delta_2 = W_R/W_{P2}$, and $\delta_3 = W_{P1}/W_{P2}$. The species R1 in the model plays the role of an activated reactant meant to replace the numerous radicals and intermediate species that are formed during a typical combustion process from reactants to products. Since it is only possible to resolve the total amount of R from the detailed chemistry results in Cantera (since R0 and R1 are chemically identical), it is assumed that the chain initiation reaction (i1) and chain branching reaction (i2) are complete when a notable amount of product species P1 and P2 begin to form. While this value is not explicitly specified by Zhu [31], we assume the initiation reaction to be complete when the combined mole fractions of the forming products are greater than or equal to 0.1 since this is found to correspond well with the start of the main exothermic reaction. Similarly, in the equilibrium region, the amount of reactant R tends to zero, since all the reactants are assumed to be consumed during the exothermic regime. Under these assumptions, the forward and backward rate constants k_{ef} and k_{er}, for the reaction (e), and the equilibrium constant, K_c, can be derived from the equilibrium regime, while the reaction rates k_{r1} and k_{r2}, for reactions (r1) and (r2), are calculated from the main exothermic regime of the ignition process. Finally, the reaction orders s_0, s_1, s_2, and s_3 are evaluated through an iterative procedure meant to provide the best possible dataset for the detailed chemistry that minimizes cumulative errors in the reaction rate parameters when fit to the predetermined functions for the reaction rates in the model. The detailed procedure for deriving the functional dependence of the rate constants in the model can be found in the original manuscript by Zhu et al. [31]. For detonation investigations, a single induction reaction existing as a packed formula with two paths, i1 and i2, was first explored by Fickett et al. [33] when studying induction zone kinetics. By assuming the ratio $k_{i1}/k_{i2} = \epsilon$ is constant such that $\epsilon \ll 1$, the production rates of the reactant species R0 and R1 can be modeled using only a single absolute rate constant, k_i. Through a high activation energy asymptotic expansion [34], it can then be shown that the absolute rate constant is inversely proportional to the ignition time for a given reactive mixture ($k_i \propto 1/\tau$). The rate

constant k_i is then modeled using constant volume process ignition time measurements from detailed chemistry.

In the Lagrangian description, the production rates for the different global species, in terms of their mass fractions, are given by

$$\begin{cases} \dfrac{\mathrm{D}Y_{\mathrm{R0}}}{\mathrm{D}t} &= -Y_{\mathrm{R0}}\left(\epsilon[\mathrm{R1}]^{s_0}\right)\cdot k_\mathrm{i} \\ \dfrac{\mathrm{D}Y_{\mathrm{R1}}}{\mathrm{D}t} &= -\dfrac{W_{\mathrm{R1}}}{W_{\mathrm{R0}}}\left(\dfrac{\mathrm{D}Y_{\mathrm{R0}}}{\mathrm{D}t}\right) \\ & \quad -\dfrac{W_{\mathrm{R1}}}{\rho}\left([\mathrm{R1}]^{s_1}\cdot k_{\mathrm{r1}} + [\mathrm{R1}]^{s_2}\cdot k_{\mathrm{r2}}\right) \\ \dfrac{\mathrm{D}Y_{\mathrm{P1}}}{\mathrm{D}t} &= \dfrac{W_{\mathrm{P1}}}{\rho}[\mathrm{R1}]^{s_1}\cdot k_{\mathrm{r1}}\cdot\delta_1 \\ & \quad -\dfrac{W_{\mathrm{P1}}}{\rho}\left([\mathrm{P1}]^{s_3}\cdot k_{\mathrm{ef}} - [\mathrm{P2}]^{s_3\delta_3}\cdot k_{\mathrm{er}}\right), \end{cases} \tag{3}$$

where [R1], [P1], and [P2] are the molar concentrations of the respective species. We note here that only three transport equations (for R0, R1, and P1) are required to be added to a system of governing equations that conserve mass, momentum, and energy for fluid motion. Unlike Zhu's formulation, we do not include an explicit transport equation for product species P2 which is an improvement in terms of memory requirements and efficiency. This simplification can be made since the sum of the mass fractions of the different species must be equal to unity ($\sum Y_\mathrm{i} = 1.0$) for any gas mixture. Thus, the mass fraction of species P2 can be readily determined. Furthermore, under the constraint that $\sum(\mathrm{D}Y_\mathrm{i}/\mathrm{D}t) = 0$, it is possible to obtain the production rate of P2 at any instant using equation set (3) if the mass fractions of the other species are known. Following the procedure above, four different stoichiometric hydrocarbon mixtures, acetylene–oxygen, methane–oxygen, propane–oxygen, and ethylene–oxygen, have been calibrated, as well as three lean acetylene–oxygen mixtures with equivalence ratios (ϕ) 0.71, 0.5, and 0.33. To verify the performance of the model across different ERMs, the acetylene mixture is calibrated using the Konnov mechanism [35], the methane mixture using the GRI-3.0 mechanism [36], and the propane and ethylene mixtures using the USC II mechanism [37]. The complete parameter sets for each of the premixed hydrocarbon mixtures investigated are available in the Appendix.

In the current study, a series of zero- and one-dimensional ignition problems are simulated over a range of initial conditions to investigate the validity of the four-step model as a suitable combustion mechanism for flame acceleration and detonation investigations. In particular, constant volume and constant pressure ignition problems as well as 1-D ZND detonations are considered. The ZND detonation model [38] is a simple one-dimensional problem which describes the steady inviscid structure of a reaction zone behind a shock wave. The model presents basic coupling of chemical reactions to steady-state gas dynamics, in the frame of reference attached to the wave. In the Lagrangian description, following the procedure outlined by Kao et al. [39], the 1-D ZND model can be expressed as a system of ordinary differential equations, with (2) coupled to respective descriptions of density, velocity, and pressure as

$$\begin{cases} \dfrac{\mathrm{D}\rho}{\mathrm{D}t} = -\rho\dfrac{\dot\sigma}{\eta} \\ \dfrac{\mathrm{D}w}{\mathrm{D}t} = w\dfrac{\dot\sigma}{\eta} \\ \dfrac{\mathrm{D}P}{\mathrm{D}t} = -\rho w^2\dfrac{\dot\sigma}{\eta}, \end{cases} \tag{4}$$

where

$$\begin{cases} \dot\sigma = \displaystyle\sum_{i=1}^{N_y}\sigma_i\frac{\mathrm{D}Y_i}{\mathrm{D}t} \\ \sigma_i = \dfrac{W}{W_i} - \dfrac{h_i}{c_pT}. \end{cases} \tag{5}$$

Here, $\dot\sigma$ is the thermicity which measures the rate at which chemical energy is transformed into thermal energy and vice versa, while ρ, P, c, h_i, and c_p, are the density, pressure, sound speed, species specific enthalpy, and mixture specific heat. The species specific enthalpy (h_i) and specific heat ($c_{p,i}$) are evaluated using the standard NASA polynomial formulation [40] as

$$\begin{cases} h_i = \dfrac{R^o}{W_i}\left(\displaystyle\sum_{n=1}^{5}\frac{a_nT^n}{n} + a_6\right) \\ c_{p,i} = \dfrac{R^o}{W_i}\displaystyle\sum_{n=1}^{5}a_nT^{n-1}, \end{cases} \tag{6}$$

where a_n represent the NASA polynomials for a given ith species in the model, while W_i and R^o are the species molecular weight and universal gas constant. The stiff system of governing equations are then solved implicitly using the Sundials CVODE solver [41] where w is the particle path velocity relative to the wave frame of reference, while $\eta = 1 - M^2$ is a sonic parameter, with M defined as the local flow mach number. For the special case of constant volume ignition, we take $(\mathrm{D}\rho/\mathrm{D}t) = (\mathrm{D}w/\mathrm{D}t) = 0.0$ and $(\mathrm{D}P/\mathrm{D}t) = -\rho c^2\dot\sigma$, while for constant pressure ignition, we take $(\mathrm{D}P/\mathrm{D}t) = (\mathrm{D}w/\mathrm{D}t) = 0.0$ and $(\mathrm{D}\rho/\mathrm{D}t) = -\rho\dot\sigma$.

3 Results

This section aims to validate the four-step model for the four hydrocarbon mixtures considered through comparison with

detailed chemistry results from Cantera [32]. Our preliminary results of the model performance in stoichiometric undiluted reactive mixtures [42] are first summarized through ignition time (τ) predictions and ZND detonation profiles. This is followed by validation of the four-step model for mixtures with varying equivalence ratios (ϕ) and dilution by an inert chemical species.

3.1 Stoichiometric undiluted reactive mixtures

Figure 1 demonstrates the agreement of ignition times (τ) predicted using the four-step model and detailed chemistry, for each reactive mixture, over a wide range of initial temperatures and densities. The ignition time (τ) is calculated as the maximum value of the derivative of temperature with respect to time, $(\mathrm{d}T/\mathrm{d}t)_{\max}$, during the complete ignition process. It is observed that the four-step model accurately recovers the detailed chemistry ignition delays for all four stoichiometric mixtures, over the entire range of initial conditions tested. We first note that the linear behavior seen in the natural logarithm of ignition delay for methane is the reason why the one-step model, with a single global activation energy, is able to reasonably capture the ignition delay times for this mixture, but not for others [43]. However, it is well known that the correct temporal evolution of temperature (or reaction stiffness) for methane is not captured with the one-step model [44]. On the other hand, for fuels like acetylene, and to a lesser extent propane and ethylene, which exhibit visible chain branching effects, independent control over the ignition time is necessary. In these cases, a single activation energy cannot correctly capture the ignition behavior over the entire temperature range.

Apart from the ignition time measurements, the four-step model does a good job at replicating the reaction, and equilibrium time scales, as well as the thermodynamic state throughout the constant volume reaction process [42]. A comparable level of accuracy is also observed between the four-step model and detailed chemistry for constant pressure ignition processes as well as the 1-D ZND detonation profiles [42]. For completeness, the ZND model results showing the temperature profiles of the reaction zone are depicted in Fig. 2 for a leading shock wave speed equal to the CJ detonation speed. The initial CJ speed for the four-step model and results for the detailed chemistry ERMs are obtained using the SD Toolbox libraries (for Cantera) [45] for an initial quiescent temperature of 300 K, and initial pressures of 1 kPa, 10 kPa, and 100 kPa. Apart from some amount of deviation observed for the ethylene mixture and the low-pressure methane case, the four-step model is observed to recover almost exactly the correct temperature profiles, and spatial scales of the reaction zone after a shock wave. These results present a big

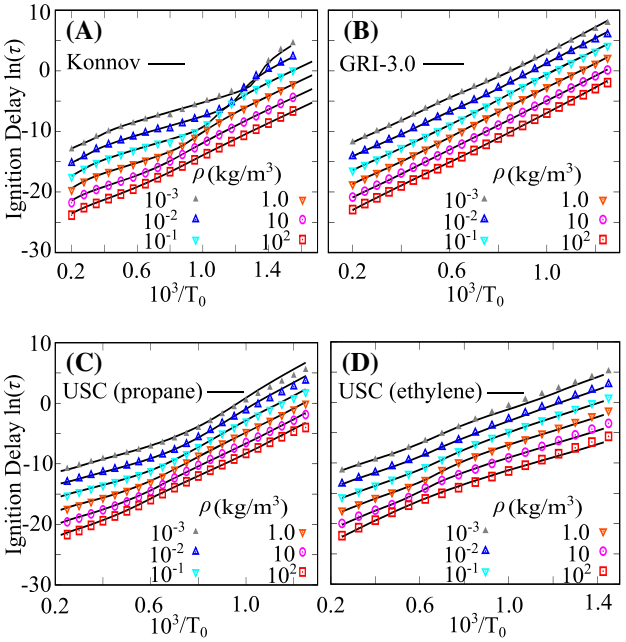

Fig. 1 Constant volume ignition time predictions of the four-step model (points) compared to the detailed chemistry mechanisms (lines) of **a** Konnov [35] for the stoichiometric acetylene–oxygen mixture, **b** GRI-3.0 [36] for the stoichiometric methane–oxygen mixture, **c** USC for the stoichiometric propane–oxygen mixture [37], and **d** USC [37] for the stoichiometric ethylene–oxygen mixture

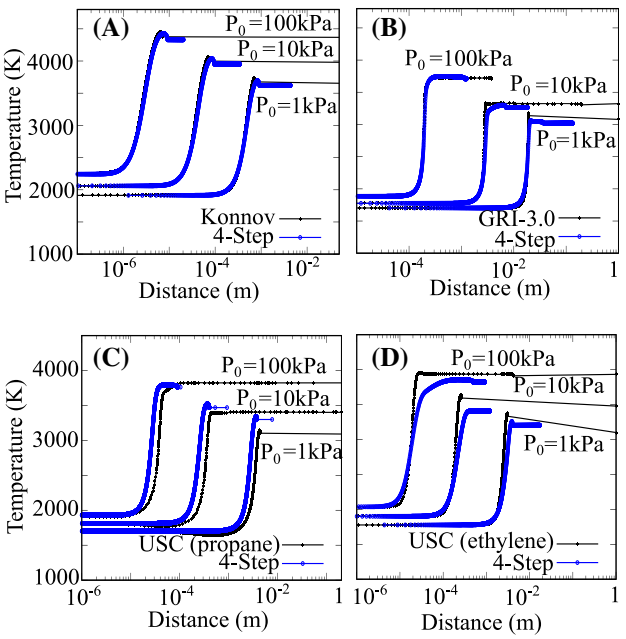

Fig. 2 Temperature profiles for ZND detonation using the four-step model (points) and detailed chemistry mechanisms (lines) for stoichiometric **a** acetylene–oxygen, **b** methane–oxygen, **c** propane–oxygen, and **d** ethylene–oxygen mixtures with $T_0 = 300$ K

improvement over other simple GRMs, such as the one-step and two-step models, which fail to capture the correct temperature profiles leading to differences in the spatial scales observed in the reaction and induction zones as well as an incorrect final equilibrium temperature.

3.2 Dilution by inert species

The influence of an inert diluent, such as argon or nitrogen, on premixed hydrocarbon detonations has been a long standing problem. It was observed that dilution of a stoichiometric acetylene–oxygen mixture by argon does not alter the activation energy (E_a) of the mixture, but is capable of altering the detonation stability and structure [46]. Past studies have concluded that this is due to a smaller amount of energy evolution per mole of the gas, with the reaction time (t_e) increasing with respect to the induction time (t_i) with increasing levels of dilution. It is then of some value to verify the performance of the four-step model for a dilute premixed reactive gas mixture, without altering the four-step model parameters determined for undiluted cases. Assuming that there are no gradients in the amount of inert diluent, the presence of the inert diluent in the model equations (3) is accounted for simply by including the mass fraction contribution as a constant global variable. There is no need for an additional transport equation since the mass fraction of inert species in the mixture remains unchanged through the reaction. To investigate the performance of the four-step model on the addition of an inert diluent, we consider two different dilute gas mixtures: 40% by volume dilution of the methane–oxygen mixture with nitrogen, and 50% by volume dilution of the acetylene–oxygen mixture with argon.

The results for the two dilute mixtures are presented in Fig. 3, noting that noticeably longer ignition time scales result from mixture dilution when compared to undiluted cases. In fact, we note that the four-step model captures very well the diluted mixture ignition delays and final equilibrium temperature when compared to the detailed chemistry simulations, without the need to re-determine the combustion model parameters for the diluted cases. From the ZND profiles, we also note that the four-step model is able to capture the correct temperature profiles to a high level of accuracy for the situations shown. The time scales and thermal states are also captured for each case.

3.3 Fuel lean mixtures

Several past studies have highlighted the influence of varying equivalence ratios (ϕ) on the flame propagation and detonation dynamics of a combustible fuel/oxygen mixture. For flames, it was observed that the flame thickness and maximum flame speed are directly influenced by the equivalence

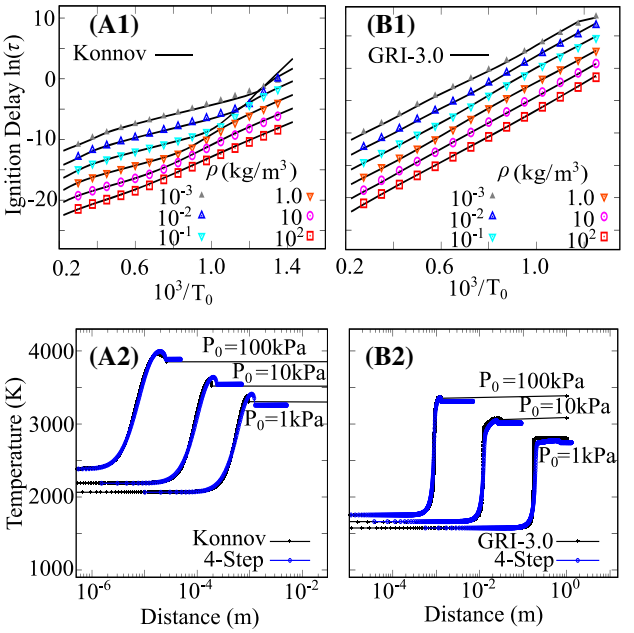

Fig. 3 Constant volume ignition time predictions and ZND detonation temperature profiles with $T_0 = 300$ K using the four-step model (points) and detailed chemistry mechanisms (lines) for **a** dilute stoichiometric acetylene–oxygen [$2C_2H_2 + 5O_2 + 7Ar$] and **b** dilute stoichiometric methane–oxygen [$CH_4 + 2O_2 + 2N_2$] mixtures

ratio [47,48], while the stable detonation velocity was found to increase as the equivalence ratio increases [49]. The variation in equivalence ratio is particularly important when studying deflagration to detonation transition (DDT) due to flame acceleration. Dorofeev et al. [50] concluded that any change in the mixture composition below stoichiometry results in a significant increase of run-up distance before transition to detonation occurs for flame acceleration in a channel with obstacles. Similarly, an equivalence ratio of about 2.0 was found to result in the shortest run-up distance as well as time to DDT from experimental results for ethylene/oxygen mixtures [49]. It is then crucial to verify the performance of the four-step model for equivalence ratios not equal to 1.0. We first note that limitations are known to exist for application of the four-step model to fuel-rich mixtures [31], which we will discuss in detail in Sect. 4.8. Thus, for now we only consider three different fuel lean acetylene mixtures with equivalence ratios equal to 0.71, 0.5, and 0.33.

The four-step model global species for fuel lean hydrocarbon mixtures ($\phi < 1.0$) are derived using (1), where the left over oxygen in the mixture is accounted for in the product species P1 and P2. Since the four-step model parameters are derived by substituting the global species into detailed chemistry results for a constant volume ignition, there is a need to derive a completely new parameter set for each unique equivalence ratio since the composition of product species P1 and P2 varies from the stoichiometric mixture. It is then

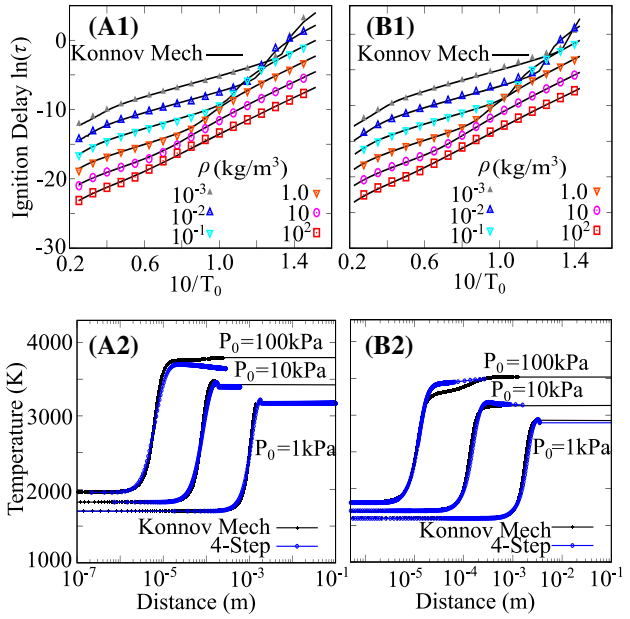

Fig. 4 Constant volume ignition time predictions and ZND detonation temperature profiles with $T_0 = 300$ K using the four-step model (points) and detailed Konnov mechanism [35] (lines) for two lean acetylene–oxygen mixtures **a** $\phi = 0.5$ and **b** $\phi = 0.33$

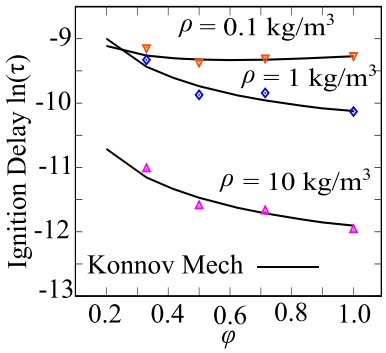

Fig. 5 Constant volume ignition delay (τ) for acetylene–oxygen mixtures as a function of equivalence ratio (ϕ) using the four-step model (points) and the detailed Konnov mechanism [35] (lines)

not possible to simply include the excess oxygen in the mixture as a global variable that remains unchanged, similar to the approach adopted for the dilute mixtures in the study. The results for two lean mixtures are shown in Fig. 4, while the complete parameter set for the mixtures is available in the Appendix. From the figures, it can be observed that the four-step model is capable of predicting the detailed mechanism temporal evolution reasonably well, with the ignition time, thermodynamic state during the exothermic reaction, and stiffness predicted to a high level of accuracy. Apart from some minor deviations observed in the final mixture equilibrium temperature profile for the ZND results, the model is observed to provide an accurate prediction of the reaction zone structure behind the leading shock wave. Finally, Fig. 5 shows a comparison of the ignition delay (τ) predicted by the four-step model and detailed chemistry as a function of the equivalence ratio (ϕ), for different initial densities, with an initial temperature of 1000 K.

4 Discussion

This section aims to determine how well the four-step model captures fundamental properties of the reactive mixture that are relevant for modeling flame acceleration, DDT [29], and also detonation wave propagation and reaction zone structures [51]. Here we compare the explosion limits, activation energies (E_a), heat release (Q), ignition time to reaction time ratios (t_i/t_e), Zel'dovich numbers (β), expansion ratios (σ), and detonation stability parameters (χ) to detailed chemistry results using Cantera. From this, we aim to determine the applicability of using the four-step model to investigate compressible and reactive flows.

4.1 Explosion limits

The explosion limits of fuel/oxidizer mixtures that separate the explosive and non-explosive regions for constant volume ignition are particularly important for demonstrating the essential role of chain branching during the ignition process. Perhaps the most well-known example of chain branching mechanisms in combustion is the "Z-shaped" non-monotonic explosion limits for hydrogen combustion, typically characterized in the pressure–temperature parameter space [52]. While small carbon chain hydrocarbon fuels, such as methane, typically demonstrate a relatively monotonic explosion curve [53], non-monotonic influences are more prominent for longer carbon chain hydrocarbons. For longer carbon chains, the chain branching mechanisms have a greater effect during ignition. For example, propane has been shown to demonstrate an "S-shaped" explosion curve in previous experiments [54]. Since the explosion curve measures the sensitivity of a reactive mixture to undergo a spontaneous ignition event, it is of great practical importance to investigate if the four-step model is capable of predicting these limits for the mixtures investigated.

Figure 6 shows the explosion limits predicted using the four-step model for stoichiometric mixtures involving acetylene, methane, propane, and ethylene and are compared to the respective explosion curves generated using the detailed chemistry mechanisms. For a constant volume ignition process, an explosion is identified if the system temperature increases by 50 K within 10 s. This explosion criteria is consistent with previous investigations [52,55]. For the ignition process, the initial pressures range from 10 to 10^7 Pa, which covers the working range of pressures in typical detonation studies, with initial temperatures ranging from

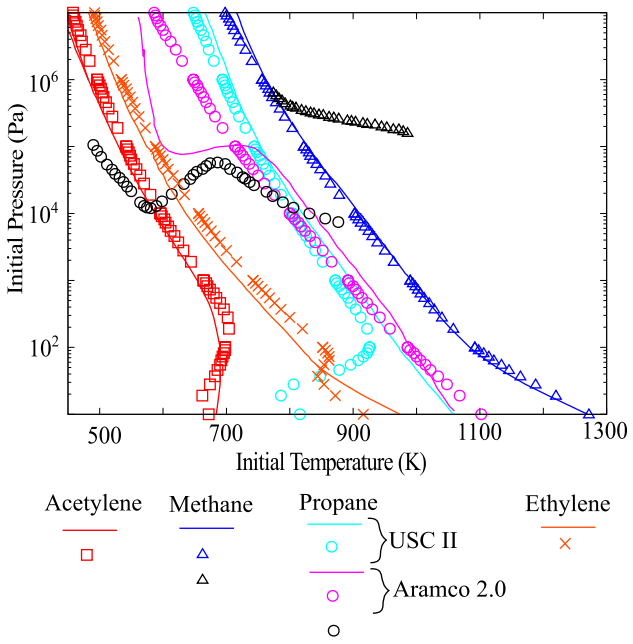

Fig. 6 Explosion limit predictions for stoichiometric acetylene–oxygen, methane–oxygen, propane–oxygen, and ethylene–oxygen using the four-step model (points) and detailed chemistry mechanisms (lines) along with experimental data points for methane [55] and propane [54] (black points)

300 to 2500 K. Apart from deviations observed in the low-pressure region, i.e., below 100 Pa, the four-step model reproduces the explosion curves for the different mixtures reasonably well on comparison with the detailed chemistry. The errors observed for low-pressure ignition ($<$ 100 Pa) can, in part, be attributed to the methodology for deriving the four-step model parameters, where calibration was only performed for initial temperatures $>$ 1000 K at low pressures [31]. This would explain why these deviations are not significant for the reactive methane mixture where the low-pressure explosion limits occur at higher temperatures.

Another key observation here is the absence of the non-monotonic chain-branching for propane at higher pressures ($>$ 1 atm) using the USC II mechanism [37], which is observed in both experiments [54] and numerically using alternate elementary reaction mechanisms, such as the Aramco 2.0 mechanism [56]. Instead, the applied detailed mechanism for propane (USC-II [37]) exhibits a relatively monotonic behavior similar to methane, and no "S-shaped" explosion limits are visible. This highlights the need for a better description of the low-temperature chain branching mechanisms for propane combustion in the USC-II mechanism [37]. To determine whether the four-step model can replicate this behavior for propane combustion, a second set of model parameters for stoichiometric–propane oxygen combustion was calibrated to the detailed Aramco 2.0 mechanism [56]. Based on the explosion curve results in Fig. 6, it appears that the four-step model is not capable of accurately replicating the non-monotonic chain branching observed at pressures $>$ 1 atm. One possible reason for this is the lack of a chain-termination reaction in the model. This reaction is well known to have a controlling influence on the explosion limits. For example, the explosion limits along the "S-shaped" explosion curve, where the curve deviates from the monotonic chain branching, are controlled by competitive mechanisms of chain branching and chain termination [57]. In the absence of any chain-termination mechanism, explosions predicted using the four-step model always proceed to consume the entire reactant. However, based on the results using the Aramco mechanism [56], this is not perceived to be significant drawback since only a maximum deviation of approximately 200 K was observed in the explosion limits where non-monotonic chain branching mechanisms are the most apparent ($>$ 1.0 atm). More importantly, based on the explosion curves for all the hydrocarbon mixtures (including the results for propane using the Aramco 2.0 mechanism), during a constant volume explosion process resulting in an increase in temperature and pressure, there exists no scenario where the reaction terminates without consuming the entire reactant as a result of the thermodynamic state progressing into the non-explosive side of the explosion curve. This is contrary to the explosion curve observed for hydrogen and is the primary reason the four-step model is not suitable for predicting hydrogen combustion. This is discussed in detail in Sect. 4.8. Based on these results, the four-step model can be expected to predict the onset of localized explosions in a numerical flow field reasonably well for the mixtures under consideration by providing the appropriate temperature and pressure-dependent ignition response.

4.2 Global activation energy (E_a) and heat release (Q)

The influence of the activation energy (E_a) on the regularity of a detonation cellular structure has been investigated heavily in the past [58]. In general, the activation energy plays the role of a control parameter in detonation systems that determines how the system responds to small disturbances, with premixed reactive mixtures with high activation energies exhibiting unstable detonation propagation with an irregular detonation structure. Similarly, the heat release directly measures the strength of pressure wave amplifications after the reaction in detonations. Predicting the correct activation energy and heat release are therefore crucial in numerical investigations of detonation waves, in order to capture the correct wave speeds and overall detonation behavior.

Figure 7 shows the results for the non-dimensional activation energy evaluated using the four-step model and Cantera for the different stoichiometric hydrocarbon mixtures, all with an initial density of $\rho = 1.0$ kg/m^3. The

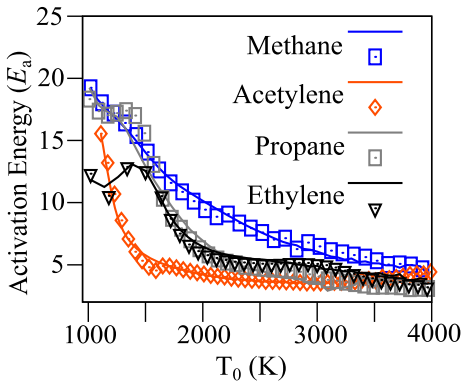

Fig. 7 Non-dimensional activation energy (E_a) for stoichiometric hydrocarbon–oxygen mixtures, all at an initial density of $\rho = 1.0\,\mathrm{kg/m^3}$ using the four-step model (points) and detailed chemistry mechanisms (lines)

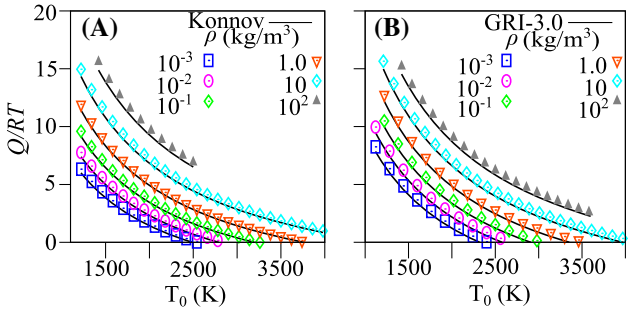

Fig. 8 Dimensionless heat release (Q/RT) predictions for stoichiometric **a** acetylene oxygen and **b** methane oxygen mixtures using the four-step model (points) and detailed chemistry mechanisms (lines)

non-dimensional activation energy (E_a/RT) for a constant volume ignition process is evaluated from

$$\frac{E_a}{RT_0} \approx \frac{1}{T_0}\frac{\ln(\tau_+) - \ln(\tau)}{1/T_{0+} - 1/T_0}, \tag{7}$$

where τ is the ignition delay time for the constant volume process with initial temperature T_0. Similarly, τ_+ corresponds to the perturbed ignition delay time for the constant volume process at an initial temperature $T_{0+} = T_0 + \Delta T$, with $\Delta = 20$ K. This value for ΔT is chosen because it is small enough to account for any change in the slope of the ignition delay measurements. The four-step model here is shown to capture the non-dimensional energy very well over the entire spectrum of initial temperatures except for minor discrepancies observed in the high-temperature ($T_0 > 3000$ K) results for the stoichiometric propane and ethylene reactive mixtures. Figure 8 shows a comparison of the dimensionless heat release (Q/RT_0) evaluated from a constant volume ignition using Cantera and the four-step model for the acetylene and methane mixtures, where R represents the gas constant and T_0 is the initial temperature. For a constant volume process occurring at a constant density, the heat release (Q) is evaluated from the change in the internal energy between the initial reactants and final (or equilibrated) products. It can be observed that the model accurately predicts the heat release value for all the density cases considered over a wide range of initial temperatures in the post-shock range. The four-step model is a significant improvement over a simple one-step model, where the activation energy (E_a) and heat release (Q) must be prescribed as model parameters and tuned to recover the correct post shock ignition delay and detonation induction length. The four-step model, on the other hand, is capable of recovering these properties automatically with a high level of accuracy.

4.3 Chapman–Jouguet (CJ) detonation velocity

The Chapman–Jouguet detonation velocity is the minimum wave speed for which there exists a steady-state solution to the reaction path-independent jump conditions in conserved mass, momentum, and energy from reactants to equilibrium products, such that the flow is sonic in the products relative to the wave speed itself. In this case, the equilibrium state is evaluated by finding the minimum Helmholtz energy in the products. Figure 9 shows the CJ detonation velocity and temperature at the CJ state, both of which are calculated using the four-step model and detailed chemistry mechanisms. The detailed chemistry solutions are obtained using the Shock and Detonation Toolbox libraries [59], while the same applied minimum-wave speed algorithm [45] is used to obtain the four-step model solutions, with the added assumption that only products P1 and P2 exist in equilibrium at the CJ state. The individual mole fractions of the product species in the final mixture are then calculated using the equilibrium function and coefficients derived as part of the four-step model parameter set for a given mixture.

To further assess the four-step model performance, Fig. 10 shows a comparison of the CJ speeds and temperatures at the CJ state for the lean acetylene–oxygen mixtures, as well as a comparison of the CJ speeds for the four different hydrocarbon mixtures at $T_0 = 300$ K and $P_0 = 1$ atm with increasing amounts of inert dilution. A very good agreement is observed between the two sets of results for all the hydrocarbon mixtures considered, with the four-step model recovering the correct CJ speed irrespective of the equivalence ratio (for $\phi \leq 1$) of and concentration of diluent. Clearly, the derived product species and equilibrium functions are valid for predicting the equilibrium thermochemistry for the different reactive hydrocarbon mixtures investigated in this study for the stoichiometric, lean, and dilute cases.

4.4 Induction-to-reaction time ratio (t_i/t_e)

A number of studies have shown that, in addition to activation energy and heat release, the detonation structure is also

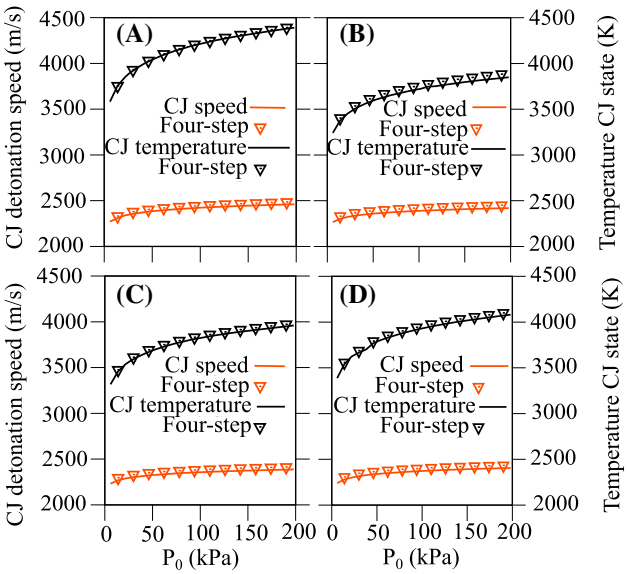

Fig. 9 CJ detonation speed and temperature predictions using the four-step model (points) and detailed chemistry mechanisms (lines) for stoichiometric **a** acetylene–oxygen, **b** methane–oxygen, **c** propane–oxygen, and **d** ethylene–oxygen mixtures with varying initial pressures and $T_0 = 300$ K

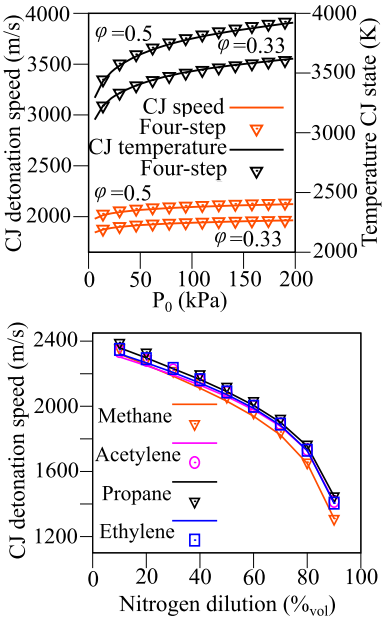

Fig. 10 CJ detonation speed and temperature predictions using the four-step model (points) and detailed chemistry mechanisms (lines) for the lean acetylene mixtures (top) and dilute hydrocarbon mixtures (bottom)

heavily influenced by the length of the induction zone (Δ_i) relative to the length of the reaction zone (Δ_e) [60]. This was first demonstrated by Short and Sharpe [61], where the stability of a one-dimensional detonation was shown to be influenced both analytically and experimentally by the ratio Δ_i/Δ_e. It was found that a thin reaction zone compared to its

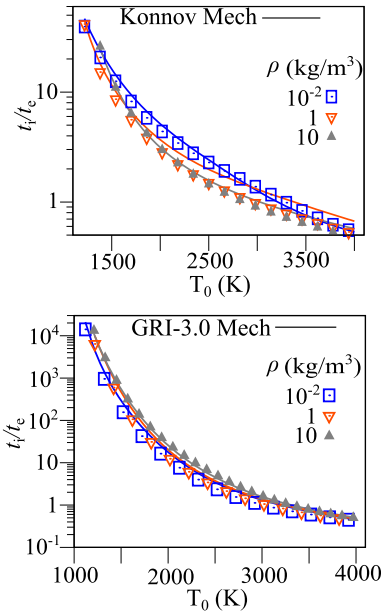

Fig. 11 Ignition time-to-reaction time ratio (t_i/t_e) predictions using the four-step model (points) and detailed chemistry mechanisms (lines) for stoichiometric acetylene–oxygen (top) and methane–oxygen mixtures (bottom)

induction zone, or a large value of Δ_i/Δ_e, has a destabilizing effect on the detonation structure due to enhanced pressure wave amplification. This is due to a large amount of energy deposited in a shorter time duration in the main reaction zone, resulting in large local heat release rates [62]. This offers one reason why a simple one-step model with no ability to independently control the ignition and reaction lengths is unable to accurately capture the ZND structure of real detonations [63]. Figure 11 shows the ignition time ratio, t_i/t_e, evaluated for constant volume reactions using both the four-step model and detailed chemistry mechanisms with varying initial densities and temperatures. Here we define the induction time (t_i) as the time to the point of maximum energy release rate, while the reaction time (t_e) is evaluated at the induction time through

$$t_e = \left(\frac{\mathrm{d}(\ln T)}{\mathrm{d}t}\right)^{-1}. \tag{8}$$

Equation (8) effectively quantifies the duration of the exothermic pulse that occurs at the end of the induction period. Since t_i/t_e does not depend significantly on density, only three density cases are for clarity. For constant volume ignition processes over the entire spectrum of initial temperatures, the four-step model predicts the correct value of t_i/t_e for most cases, and never deviates beyond the correct order of magnitude.

4.5 Detonation stability and the χ parameter

For detonation wave propagation, the non-dimensional χ-parameter, given by

$$\chi = \frac{t_i}{t_e}\left(\frac{E_a}{RT_{vn}}\right)\left(\frac{Q}{RT_{vn}}\right), \tag{9}$$

can be used to predict whether a reactive mixture is particularly prone to instabilities since it measures directly the propensity for disturbances to amplify from hot spot ignition. χ is simply the product of the ratios of characteristic induction and reaction times (t_i/t_e), the non-dimensional activation energy (E_a/RT_{vn}), and non-dimensional heat released during the reaction (Q/RT_{vn}) of the post-shocked reactive mixture. The precise role of the χ parameter has been investigated in past studies [19,51,60,64], with a critical $\chi \approx 50-100$ correlating well with the onset of cellular instabilities. It was also found that mixtures with high χ values will develop highly unstable detonations due to rapid amplification of gas dynamic disturbances in the reaction zone. More recently, for detonation propagation into reactive layers bounded by an inert gas [65], it was suggested that the χ parameter is important for determining the critical height of the reactive layer after which detonation propagation is no longer possible. In this investigation, simulations that used detailed chemistry mechanisms were observed to have much larger χ parameter values compared to simulations with simpler combustion models. Consequently, the detonation wave simulated using detailed chemistry developed larger cellular instabilities for smaller reactive layer widths and was quenched at a much smaller critical height.

Following the procedure outlined in [64], the χ parameter values were evaluated from constant volume ignition problems for a wide range of initial post-shock (von Neumann) temperatures using both detailed chemistry and the four-step model. In Fig. 12, the χ values are shown first for the different stoichiometric mixtures, and then for the acetylene oxygen mixtures for different levels of argon dilution, all for $\rho = 1.0$ kg/m^3. As observed, the four-step model provides a reasonably accurate prediction of the χ value calculated using Cantera over the entire range of post-shock temperatures. Additionally, the results for the stoichiometric mixtures are also in line with past experimental studies [19,66], with the stoichiometric methane mixture exhibiting the most unstable, or irregular, cellular structure (the largest χ value) and the most stable detonation cellular structure is observed for acetylene. The addition of an inert diluent like argon has been shown to affect the stability and detonation structure due to an increase in the reaction length (Δ_e), with mixtures diluted by argon exhibiting more stable, or regular, cellular structures when compared to undiluted mixtures [58]. This behavior of the χ parameter decreasing with

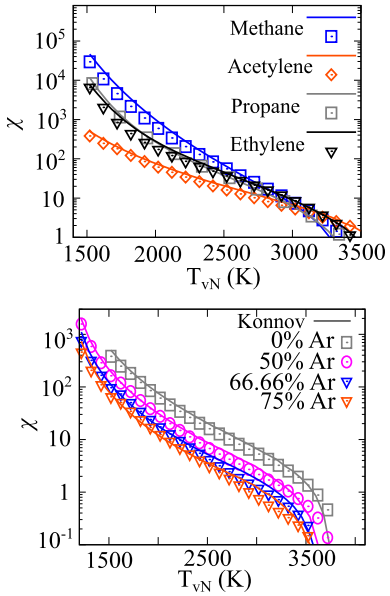

Fig. 12 Dimensionless χ parameter predictions using the four-step model (points) and detailed chemistry mechanisms (lines) for the four different hydrocarbon mixtures (top) and dilute acetylene–oxygen mixtures (bottom)

increasing amounts of a diluent is clearly visible in Fig. 12b. Based on these results, we can expect that the four-step model is well-suited for simulating the multidimensional detonation propagation behavior and cellular structure, including local quenching and re-initiation behavior during propagation.

4.6 Expansion ratio (σ) and the Zel'dovich number (β)

Finally, since flame propagation is an important component feature of detonation waves, i.e., through its initiation via DDT, or even the burn up of unburned pockets in a detonations wake during propagation [44], it is also important to analyze corresponding key features associated with the chemical mechanism. Flames are often characterized using the laminar flame speed and thickness. In the limit of large activation energy, the problem of laminar flame propagation reduces to an eigen value problem with one solution for the laminar flame speed S_L [67]. As outlined by Zel'dovich et al. [68], the laminar flame speed is found to depend on three dimensionless parameters, the expansion ratio (σ), Zeldovich number (β), and Lewis number (Le) [29]. The expansion ratio is the ratio of unburned reactant density to the density of the burned products for a constant pressure process, i.e., $\sigma = \rho_u/\rho_b$, while the Lewis number is the ratio of thermal diffusivity to the mass diffusivity. Finally, the Zel'dovich number is calculated from

$$\beta = \frac{E_a(T_b - T_u)}{RT_b^2}, \tag{10}$$

where T_u and T_b are the temperatures of the unburned reactants and burnt products, respectively, for a constant pressure ignition process, while E_a is evaluated at T_b, and R the mixture gas constant.

Past research has highlighted the influence these dimensionless parameters have on the response of a combustion process to flow disturbances, particularly on the flame acceleration process and transition to detonation [69–71]. Since the expansion ratio (σ) physically represents how much a fluid particle will expand when it combusts, a larger expansion ratio results in a stronger flame acceleration. Furthermore, Dorofeev et al. [70] noted that a large expansion ratio is a key parameter for the onset of significant flame acceleration in experiments with repeated obstacles inside a tube. Similarly, the Zel'dovich number (β) is indicative of the flame sensitivity to thermodynamic perturbations, with larger values corresponding to a greater reaction time variation for a given change in temperature. For flame acceleration of hydrocarbon mixtures in smooth channels and channels with obstructions [29], it has been observed that the critical expansion ratio (σ_c) that separates a slow flame from chocked flames and detonations increases with an increase in β. Lastly, Le is indicative of the characteristic heat transfer in a mixture relative to the diffusion of the rate limiting species, with a smaller Lewis number favorable for flame propagation. It is then essential that the four-step model predicts these parameters accurately to correctly calculate the flow kinetics and thermodynamics when investigating DDT in channels, flame acceleration processes, and transition to detonation after shock–flame interactions. To couple the four-step model equations to a Navier–Stokes framework CFD solver, the diffusion coefficients, and consequently Le, need to be carefully calibrated to capture the correct laminar burning velocity (S_L). However, this is beyond the scope of the current study which focuses on capturing the developing chemical details accurately. We will then focus on evaluating the four-step model performance at recovering the expansion ratios and Zel'dovich numbers, acquired directly from the combustion process, when compared to the results from detailed chemistry mechanisms.

Figures 13 and 14 summarize the results for the expansion ratios and Zel'dovich numbers. To calculate σ, ρ_b is evaluated by equilibrating the reactive mixture at constant pressure and enthalpy, while the global activation energy for β was calculated using (7) from a constant volume process, with T_0 equal to the final temperature of the constant pressure ignition, T_b. This is consistent with previous documented work of Bane et al. [72]. It was observed that for a given initial pressure, the values of σ overlapped closely for the different hydrocarbon mixtures over the entire range of initial temperatures. For the sake of clarity, the results in Fig. 13 show a comparison of the expansion ratio predicted by the four-step model for three different initial pressures for the stoichiometric acetylene and methane mixtures, with the model capturing the correct density values during the complete ignition process over the entire spectrum of initial temperatures for all constant pressure ignition processes. Similarly, the Zel'dovich numbers for initial pressures equal to 1 atm and 10 atm are shown in Fig. 14. On comparison between the two sets of results, β is found to be captured reasonably well over the entire range of initial temperatures for the four different stoichiometric hydrocarbon mixtures. Finally, since the four-step model has been shown in Sect. 3 to predict the overall reaction stiffness accurately (i.e., the temperature evolution), there should be no need for tuning of the diffusion coefficients. This addresses a significant limitation of the one-step model, where there is a need to calibrate the diffusion coefficients to recover the correct laminar flame speed due to inaccurate modeling of the temperature and species gradients. The diffusion coefficients for the four-step model can likely be acquired directly from Cantera [32] using the appropriate chemistry mechanism and transport model. In this regard, the four-step model should also reproduce well the Lewis numbers at varying conditions. Based on this, and the results above, the model can be expected to predict the laminar flame speed well on comparison with detailed chem-

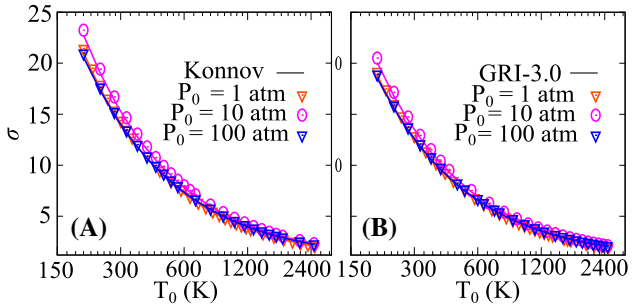

Fig. 13 Expansion ratio (σ) predictions using the four-step model (points) and detailed chemistry mechanisms (lines) for the stoichiometric **a** acetylene–oxygen and **b** methane–oxygen mixtures for varying initial pressures

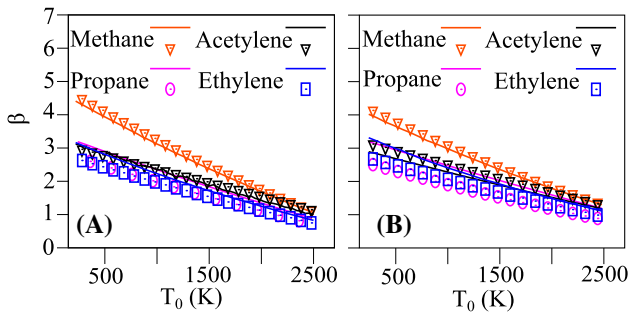

Fig. 14 Zel'dovich number (β) predictions using the four-step model (points) and detailed chemistry mechanisms (lines) for the four different stoichiometric hydrocarbon mixtures with **a** $P_0 = 1$ atm and **b** $P_0 = 10$ atm

istry which is crucial for deflagration to detonation transition investigations.

4.7 Error measurements

In order to fully evaluate the performance of the four-step model, a quantitative error analysis is carried out for the results presented. The agreement between the four-step model and detailed chemistry is investigated using an error function recently applied by Hu et al. [73], which is an improved error evaluation method over previously applied methods [74]. The error function in the current study can be summarized as:

$$\begin{cases} E_i = \dfrac{1}{N_i}\displaystyle\sum_{j=1}^{N_i}\left(\left|\dfrac{Y_{ij}^{\text{model}} - Y_{ij}^{\text{ERM}}}{\overline{Y_{ij}^{\text{ERM}}}}\right|\right) \\ E = \dfrac{1}{N}\displaystyle\sum_{i=1}^{N} E_i \\ \text{where:} \\ Y_{ij} = y_{ij} \end{cases} \tag{11}$$

Here E is the error value for N number of datasets analyzed, while E_i corresponds to the error value of the ith dataset with N_i data points; Y_{ij}^{model} and Y_{ij}^{ERM} represent the results of interest for the four-step model and detailed chemistry, respectively, for the jth data point in the ith dataset, while $\overline{Y_{ij}^{\text{ERM}}}$ is the average measurement of the ith dataset. Normalizing the error with the number of data points (N_i) prevents bias toward datasets with a large number of points, and considering the average is necessary to prevent bias toward measured data points where the error is the largest. The model is considered to be correctly predicting the datum (i.e., the detailed chemistry result) when E has a value between 0 and 1 [73,75].

Figure 15 summarizes the error function measurements for the four different stoichiometric hydrocarbon mixtures under investigation for the different parameters compared throughout this paper. The datasets selected for the error calculation of each measured parameter cover the entire spectrum of initial temperatures, densities, and pressures for detonations. As observed, the error value for all measurements is below 0.35. Moreover, the largest errors are observed for parameters that include multiple components, namely the induction-to-reaction time ratio (t_i/t_e), detonation χ parameter, and β. The results are particularly impressive for the natural logarithm of the induction time (τ), normalized E_a, CJ speeds, and expansion ratios, with error function values less than 0.1.

4.8 Model limitations

The primary limitation of the four-step model is its inability to account for situations where unreacted fuel is present in the final equilibrium mixture of a constant volume ignition process [31]. This makes the model unsuitable for investigating combustion in fuel-rich hydrocarbon mixtures ($\phi > 1.0$) and also ignition processes where the chain-branching is highly non-monotonic, such as for hydrogen combustion. For example, stoichiometric hydrogen–oxygen mixtures were found to contain approximately 10–20% of hydrogen fuel by volume, in cases where the combustion ends up outside of the explosion curve and the remaining reactant is not consumed. The current methodology requires that there is no fuel present in the products after ignition in order to derive the functions that describe the concentration of the product species after ignition. The leftover fuel cannot simply be included in the product groups (P1 and P2) due to their unstable nature and their complicated dissociation and recombination processes at elevated temperatures [31]. To account for situations where unreacted fuel is present in the equilibrium mixture would require revision of the model to account for an additional product species (the leftover reactant) having independent equilibrium reactions with P1 and P2. This would increase the complexity and computational expense of the model. Excess oxygen, on the other hand, was found to be easier to incorporate into the product species for fuel lean mixtures. As highlighted in Sect. 2, the equilibrium rate constants (k_{ef} and k_{er}) are derived from a constant volume process under the assumption that the total amount of reactant R tends to zero after the exothermic reaction. Since the exothermic reaction rate constants (k_{r1} and k_{r2}) depend on the values of the equilibrium rate constants, the model is then incapable of characterizing the developing details during the main heat release reaction accurately for these cases. When modeling of a stoichiometric hydrogen–oxygen ignition process was attempted, errors as large as 40% were observed in the final equilibrium temperature and pressure.

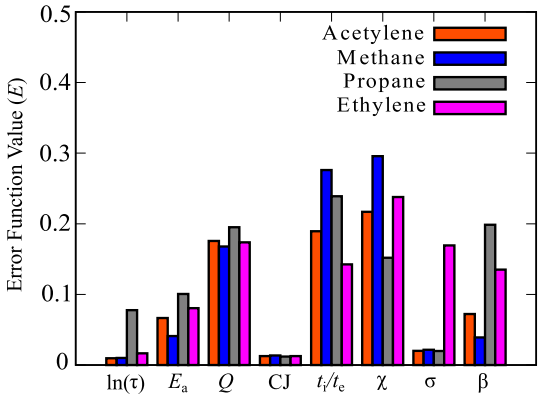

Fig. 15 Error function (E) results for the four-step model for ignition time predictions (τ), non-dimensional activation energy (E_a), non-dimensional heat release (Q), CJ speed, induction time-to-reaction time ratio (t_i/t_e), detonation χ parameter, expansion ratio (σ), and Zel'dovich number (β) for the four different stoichiometric hydrocarbon mixtures under consideration

Finally, the four-step model assumption of a thermally neutral chain branching mechanism, and no dissociation reaction, cannot reproduce the endothermic behavior exhibited by some reactive hydrocarbon mixtures prior to ignition at higher temperatures, see [42]. Since dissociation reactions are typically endothermic in nature, this temperature decrease is attributed to the formation of radicals in the induction regime, that are not accounted for in the four-step model. Additional investigation is needed to properly understand the phenomenon, with the possible need to alter the chain initiation and branching equations in (2) to include additional radicals and thermodynamic states that could be produced in these cases. This, however, is not perceived to be a significant issue with the current methodology. The model recovers well the fundamental parameters investigated in this section, even for cases that exhibit this endothermic behavior.

5 Conclusion

In this study, a detailed investigation of a four-step combustion model [31] was carried out, through comparison with detailed chemistry results, in order to assess the validity of using the approach to model compressible and reactive flows (i.e., flame acceleration, and flows involving detonations). Through the thermochemical approach of replicating the performance of a detailed chemistry mechanism, the four-step model is found to provide a very good approximation of the thermodynamic properties expected for a wide range of conditions for several reactive hydrocarbon mixtures. The independent tuning of the length and time scales in the reaction and induction zones leads to an accurate estimation of the overall reaction stiffness (i.e., temperature evolution) during the combustion process. This is particularly important for applications like modeling DDT, where the flame acceleration and transition to detonation occur over vastly different length and time scales, and where the unreacted temperatures and pressures constantly change. Additionally, with the four-step model only requiring three supplementary transport equations to explain the developing chemistry details, it is a computationally inexpensive mechanism that can be efficiently coupled with CFD codes. Since the trade-off between accuracy and computational expense remains a dilemma when solving highly stiff detonation scenarios numerically, the four-step model results demonstrate a significant improvement in accuracy over other simpler idealized GRMs for reactive hydrocarbon mixtures. This advantage of requiring very little CPU overhead or memory requirements can permit higher resolutions to be attained compared to using detailed chemical models.

The four-step model is capable of reproducing important mixture properties associated with flame acceleration and detonation dynamics, namely the global activation energy, heat release, CJ velocity, induction-to-reaction time ratio, Zel'dovich number, χ parameter, and expansion ratio. With the model accurately recovering these parameters, and never deviating beyond the correct order of accuracy, we can expect good performance and accuracy when coupled to a Navier–Stokes solver. Alternate applications of the four-step model include modeling combustion for very long chain hydrocarbons such as jet-fuel surrogates and oxygenated fuels (alcohols and ethers). Although a thorough analysis of the applicability of the model for these reactive mixtures is out of the scope of the current study and left for future investigation, preliminary results indicate that the equilibrium mixtures of these fuels after combustion do indeed exhibit a degree of regularity in composition which is needed to formulate the species in the four-step model. As a result, the four-step model is expected to predict the initial and terminal states of the combustion in these fuels reasonably well. The four-step combustion model investigated here is well suited to investigate a variety of compressible and reactive flows in hydrocarbon mixtures. Such applicable flows would include flame acceleration and transition to detonation, detonation cellular dynamics, detonation quenching and re-initiation limits, and DDT via shock–flame interactions. Finally, it is also worth highlighting that the procedure for calibrating the four-step model is unchanged across different chemistry mechanisms and reactive mixtures. Since detailed chemistry mechanisms are continually developed to include more recent experiments, re-calibrating the model parameters to include these changes is trivial and we anticipate no loss in the model's accuracy.

Appendix 1: Important model equations

$\rightarrow$ Equilibrium mole fraction

$$\begin{cases} \lambda_{\mathrm{eP1}} = \left(1 + \exp[-\eta \cdot (\beta_0 + \beta_1 \cdot \eta + \beta_2 \cdot \eta^2)]\right)^{-1} \\ \lambda_{\mathrm{eP2}} = 1.0 - \lambda_{\mathrm{eP1}} \end{cases}$$

where $\eta = \dfrac{10^2 \cdot \xi - (\alpha_1 + \alpha_2 \cdot \theta)}{\delta_0 + \delta_1 \cdot \theta + \delta_2 \cdot \theta^2}$; $\theta = \ln \rho$; $\xi = 10^3/T\,(\mathrm{K})$; α, β, δ are the equilibrium relation coefficients.

$\rightarrow$ Equilibrium constant (K_c)

$$\begin{cases} K_\mathrm{c} = \left(\dfrac{[\mathrm{P2}]_\mathrm{e}^{\delta_3}}{[\mathrm{P1}]_\mathrm{e}}\right)^{1/s_3} \\ \text{where} : [\mathrm{X}]_\mathrm{e} = \lambda_{\mathrm{eX}} \cdot \dfrac{\rho_{\mathrm{P1}} + \rho_{\mathrm{P2}}}{W_{\mathrm{P1}} + W_{\mathrm{P2}}} \end{cases}$$

W_X: species molecular weight; $[\mathrm{X}]_\mathrm{e}$: species equilibrium molar concentration.

→ Rate constants for reaction (e)

$$\begin{cases} k_{\mathrm{ef}} = A \cdot \rho^m \cdot T^n \cdot \exp\left(\dfrac{E_\mathrm{a} \cdot T_0}{T}\right) \\ k_{\mathrm{er}} = k_{\mathrm{ef}}/K_\mathrm{c} \\ \text{where : } T_0 = 298.0\ \mathrm{K} \end{cases}$$

A, m, n, E_a: constants from the curve fitting procedure.

→ Rate constants for reactions (r1) and (r2)

$$\begin{cases} k_{\mathrm{r1}} = \phi_{r1} \cdot k_{\mathrm{r1H}} + (1 - \phi_{r1}) \cdot k_{\mathrm{r1L}} \\ k_{\mathrm{r2}} = \phi_{r2} \cdot k_{\mathrm{r2H}} + (1 - \phi_{r2}) \cdot k_{\mathrm{r2L}} \\ k_{\mathrm{rH}} = A \cdot \rho^m \cdot T^n \cdot \exp\left(\dfrac{E_\mathrm{a} \cdot T_0}{T}\right) \\ k_{\mathrm{rL}} = A \cdot \rho^m \cdot T^n \cdot \exp\left(\dfrac{E_\mathrm{a} \cdot T_0}{T}\right) \\ \text{where : } \phi = \left(1 + \exp(\mu \cdot (\xi - \xi_\mathrm{c}))\right)^{-1} \end{cases}$$

ϕ: transit function; μ: transit function slope; ξ_c: value of ξ where $\phi = 0.5$.

→ Rate constant for reactions (i1) and (i2)

$$\begin{cases} k_\mathrm{i} = \phi_i \cdot k_{\mathrm{iH}} + (1 - \phi_i) \cdot k_{\mathrm{iL}} \\ k_{\mathrm{iH}} = A \cdot \rho^m \cdot T^n \cdot \exp\left(\dfrac{E_\mathrm{a} \cdot T_0}{T}\right) \\ k_{\mathrm{iL}} = A \cdot \rho^m \cdot T^n \cdot \exp\left(\dfrac{E_\mathrm{a} \cdot T_0}{T}\right) \\ \text{where : } \phi = \left(1 + \exp(\mu \cdot (\xi - \xi_\mathrm{c}))\right)^{-1} \end{cases}$$

Appendix 2: Model parameters

Following the nomenclature adopted by Zhu [31], the model parameters for the different hydrocarbons are summarized in this section.

A.2.1 Stoichiometric acetylene–oxygen mixture

Reactants: $2C_2H_2 + 5O_2$
Mechanism: Konnov [35]
Equilibrium relation coefficients:

$$\begin{cases} \alpha_1 = 26.966 & \alpha_2 = -1.7044 \\ \beta_0 = 3.7136 & \beta_1 = -1.4730 \\ \beta_2 = 1.0328 & \delta_0 = 15.7345 \\ \delta_1 = 0.2625 & \delta_2 = 0.0048 \end{cases}$$

Reaction orders:

$$\begin{cases} s_0 = 0.339 & s_1 = 0.867 \\ s_2 = 0.867 & s_3 = 1.09 \end{cases}$$

$$k_{\mathrm{ef}} = 2.88 \times 10^{30} \rho^{0.925} T^{-4.826} \cdot \exp\left(\frac{-235.76 T_0}{T}\right)$$

$$k_{\mathrm{r1}} \begin{cases} k_{\mathrm{r1H}} = 1.31 \times 10^9 \rho^{1.081} \cdot \exp\left(\dfrac{-26.91 T_0}{T}\right) \\ k_{\mathrm{r1L}} = 1.339 \times 10^9 \rho^{1.084} \cdot \exp\left(\dfrac{-43.56 T_0}{T}\right) \\ \mu_{\mathrm{r1}} = 50.0; \quad \xi_{\mathrm{c1}} = 0.115 + \dfrac{0.088}{\rho^{0.1}} \end{cases}$$

$$k_{\mathrm{r2}} \begin{cases} k_{\mathrm{r2H}} = 1.394 \times 10^9 \rho^{1.087} \cdot \exp\left(\dfrac{-32.2 T_0}{T}\right) \\ k_{\mathrm{r2L}} = 8.298 \times 10^8 \rho^{1.071} \cdot \exp\left(\dfrac{-47.67 T_0}{T}\right) \\ \mu_{\mathrm{r2}} = 45.0; \quad \xi_{\mathrm{c2}} = 0.1296 + \dfrac{0.096}{\rho^{0.1}} \end{cases}$$

$$k_\mathrm{i} \begin{cases} k_{\mathrm{iH}} = & 1.127 \times 10^{-2} \rho^{0.658} T^{2.94} \\ & \cdot \exp\left(\dfrac{-11.24 T_0}{T}\right) \\ k_{\mathrm{iL}} = & 8.298 \times 10^8 \rho^{1.071} \cdot \exp\left(\dfrac{-47.67 T_0}{T}\right) \\ \mu_\mathrm{i} = & 0.0028\rho^5 + 0.01038\rho^4 - 0.054619\rho^3 \\ & +0.4165\rho^2 - 3.0473\rho + 20.00 \\ \xi_{\mathrm{ci}} = & 0.0002654588\rho^3 + 0.0010179\rho^2 \\ & -0.0753064\rho + 0.80079 \end{cases}$$

A.2.2 Stoichiometric methane–oxygen mixture

Reactants: $CH_4 + 2O_2$
Mechanism: GRI-3.0 [36]
Equilibrium relation coefficients:

$$\begin{cases} \alpha_1 = 25.4105 & \alpha_2 = -1.7502 \\ \beta_0 = 3.7696 & \beta_1 = -0.9962 \\ \beta_2 = 0.4663 & \delta_0 = 14.457 \\ \delta_1 = 0.28865 & \delta_2 = 0.00686 \end{cases}$$

Reaction orders:

$$\begin{cases} s_0 = 0.3727 & s_1 = 0.724 \\ s_2 = 0.724 & s_3 = 1.026 \end{cases}$$

$$k_{\mathrm{ef}} = 2.645 \times 10^{33} \rho^{0.9726} T^{-5.471} \cdot \exp\left(\frac{-244.5 T_0}{T}\right)$$

$$k_{r1}\begin{cases} k_{r1H} = 1.414\times10^{10}\rho^{1.267}\cdot\exp\left(\dfrac{-58.48T_0}{T}\right) \\ k_{r1L} = 2.394\times10^{9}\rho^{1.304}\cdot\exp\left(\dfrac{-55.65T_0}{T}\right) \\ \mu_{r1} = 26.632; \quad \xi_{c1} = 0.279 + \dfrac{0.048}{\rho^{0.1}} \end{cases}$$

$$k_{r2}\begin{cases} k_{r2H} = 5.056\times10^{9}\rho^{1.266}\cdot\exp\left(\dfrac{-59.98T_0}{T}\right) \\ k_{r2L} = 1.124\times10^{9}\rho^{1.308}\cdot\exp\left(\dfrac{-61.49T_0}{T}\right) \\ \mu_{r2} = 25.74; \quad \xi_{c2} = 0.3107 + \dfrac{0.0282}{\rho^{0.1}} \end{cases}$$

$$k_{i}\begin{cases} k_{iH} = 8.555\times10^{11}\rho^{0.621}T^{-0.6011} \\ \qquad \cdot\exp\left(\dfrac{-68.967T_0}{T}\right) \\ k_{iL} = 9.908\times10^{8}\rho^{0.4269}\cdot\exp\left(\dfrac{-68.9189T_0}{T}\right) \\ \mu_{i} = -0.000451\rho^5 + 0.00222\rho^4 + 0.06997\rho^3 \\ \qquad -0.2004\rho^2 - 1.878\rho + 11.00 \\ \xi_{ci} = 0.00035647\rho^3 - 0.003383\rho^2 \\ \qquad -0.0513858\rho + 0.52555 \end{cases}$$

A.2.3 Stoichiometric propane–oxygen mixture

Reactants: $C_3H_8 + 5O_2$
Mechanism: USC II [37]
Equilibrium relation coefficients:

$$\begin{cases} \alpha_1 = 25.87966 & \alpha_2 = -1.735998 \\ \beta_0 = 2.2067 & \beta_1 = -0.47167 \\ \beta_2 = 0.1751 & \delta_0 = 9.11008 \\ \delta_1 = 0.18916 & \delta_2 = 0.003929 \end{cases}$$

Reaction orders:

$$\begin{cases} s_0 = 0.339 & s_1 = 0.85 \\ s_2 = 0.85 & s_3 = 1.01 \end{cases}$$

$$k_{ef} = 2.284\times10^{27}\rho^{0.986}T^{-4.051}\cdot\exp\left(\frac{-221.1T_0}{T}\right)$$

$$k_{r1}\begin{cases} k_{r1H} = 2.925\times10^{9}\rho^{1.065}\cdot\exp\left(\dfrac{-47.53T_0}{T}\right) \\ k_{r1L} = 3.122\times10^{9}\rho^{0.9339}\cdot\exp\left(\dfrac{-53.09T_0}{T}\right) \\ \mu_{r1} = 61.895; \quad \xi_{c1} = 0.234 + \dfrac{0.0777}{\rho^{0.1}} \end{cases}$$

$$k_{r2}\begin{cases} k_{r2H} = 2.126\times10^{9}\rho^{1.116}\cdot\exp\left(\dfrac{-58.63T_0}{T}\right) \\ k_{r2L} = 8.351\times10^{8}\rho^{0.928}\cdot\exp\left(\dfrac{-52.58T_0}{T}\right) \\ \mu_{r2} = 17.029; \quad \xi_{c2} = 0.2286 + \dfrac{0.0648}{\rho^{0.1}} \end{cases}$$

$$k_{i}\begin{cases} k_{iH} = 2997445.79311\times10^{9}\rho^{.625}T^{0.522} \\ \qquad \cdot\exp\left(\dfrac{-31.508T_0}{T}\right) \\ k_{iL} = 45563\times10^{8}\rho^{0.43307} \\ \qquad \cdot\exp\left(\dfrac{-67.1979T_0}{T}\right) \\ \mu_{i} = 0.00183\rho^5 + 0.0099\rho^4 - 0.0758\rho^3 \\ \qquad -0.4527\rho^2 + 0.3503\rho + 26.12 \\ \xi_{ci} = -0.00016686\rho^3 - 0.00219299\rho^2 \\ \qquad -0.024983\rho + 0.578888 \end{cases}$$

A.2.4 Stoichiometric ethylene–oxygen mixture

Reactants: $C_2H_4 + 3O_2$
Mechanism: USC II [37]
Equilibrium relation coefficients:

$$\begin{cases} \alpha_1 = 26.19335 & \alpha_2 = -1.72655 \\ \beta_0 = 3.391898 & \beta_1 = -1.13166 \\ \beta_2 = 0.694805 & \delta_0 = 14.2155 \\ \delta_1 = 0.25896 & \delta_2 = 0.0045767 \end{cases}$$

Reaction orders:

$$\begin{cases} s_0 = 0.339 & s_1 = 0.724 \\ s_2 = 0.724 & s_3 = 1.02 \end{cases}$$

$$k_{ef} = 2.323\times10^{38}\rho^{0.9957}T^{-6.805}\cdot\exp\left(\frac{-254.1T_0}{T}\right)$$

$$k_{r1}\begin{cases} k_{r1H} = 3.706\times10^{9}\rho^{1.238}\cdot\exp\left(\dfrac{-45.43T_0}{T}\right) \\ k_{r1L} = 5.521\times10^{9}\rho^{1.164}\cdot\exp\left(\dfrac{-54.99T_0}{T}\right) \\ \mu_{r1} = 63.7757; \quad \xi_{c1} = 0.1959 + \dfrac{0.1302}{\rho^{0.10998}} \end{cases}$$

$$k_{r2}\begin{cases} k_{r2H} = 1.536\times10^{9}\rho^{1.234}\cdot\exp\left(\dfrac{-47.42T_0}{T}\right) \\ k_{r2L} = 4.42\times10^{9}\rho^{1.158}\cdot\exp\left(\dfrac{-60.09T_0}{T}\right) \\ \mu_{r2} = 19.3347; \quad \xi_{c2} = 0.2156 + \dfrac{0.03279}{\rho^{0.30459}} \end{cases}$$

$$k_{\mathrm{i}}\begin{cases} k_{\mathrm{iH}} = & 9.0615\times10^{3}\rho^{0.595}T^{1.3167} \\ & \cdot\exp\left(\dfrac{-32.152T_0}{T}\right) \\ k_{\mathrm{iL}} = & 3.34\times10^{7}\rho^{0.615}\cdot\exp\left(\dfrac{-38.99T_0}{T}\right) \\ \mu_{\mathrm{i}} = & 0.00322\rho^5+0.01779\rho^4-0.2355\rho^3 \\ & -1.226\rho^2+4.1982\rho+33.0 \\ \xi_{\mathrm{ci}} = & -0.000584\rho^3-0.00589\rho^2 \\ & -0.01446499\rho+0.606825 \end{cases}$$

A.2.5 Lean acetylene–oxygen mixture ($\phi = 0.714$)

Reactants: $2C_2H_2 + 7O_2$
Mechanism: Konnov [35]
Equilibrium relation coefficients:

$$\begin{cases} \alpha_1 = 25.93548 & \alpha_2 = -1.7119 \\ \beta_0 = 3.2895 & \beta_1 = -0.71475 \\ \beta_2 = 0.727578 & \delta_0 = 12.785428 \\ \delta_1 = 0.23094 & \delta_2 = 0.0053167 \end{cases}$$

Reaction orders:

$$\begin{cases} s_0 = 0.334 & s_1 = 0.867 \\ s_2 = 0.867 & s_3 = 1.09 \end{cases}$$

$$k_{\mathrm{ef}} = 3.507\times10^{31}\rho^{0.9292}T^{-5.098}\cdot\exp\left(\frac{-239.8T_0}{T}\right)$$

$$k_{\mathrm{r1}}\begin{cases} k_{\mathrm{r1H}} = 9.907\times10^{9}\rho^{0.99}\cdot\exp\left(\dfrac{-60.36T_0}{T}\right) \\ k_{\mathrm{r1L}} = 1.114\times10^{9}\rho^{1.098}\cdot\exp\left(\dfrac{-39.5T_0}{T}\right) \\ \mu_{\mathrm{r1}} = 40.1457; \quad \xi_{\mathrm{c1}} = 0.2481+\dfrac{0.0793}{\rho^{0.1}} \end{cases}$$

$$k_{\mathrm{r2}}\begin{cases} k_{\mathrm{r2H}} = 5.847\times10^{9}\rho^{0.982}\cdot\exp\left(\dfrac{-61.00T_0}{T}\right) \\ k_{\mathrm{r2L}} = 1.057\times10^{9}\rho^{1.054}\cdot\exp\left(\dfrac{-48.99T_0}{T}\right) \\ \mu_{\mathrm{r2}} = 75.4195; \quad \xi_{\mathrm{c2}} = 0.2463+\dfrac{0.0333}{\rho^{0.1}} \end{cases}$$

$$k_{\mathrm{i}}\begin{cases} k_{\mathrm{iH}} = & 5.163\rho^{0.707}T^{2.245}\cdot\exp\left(\dfrac{-18.83T_0}{T}\right) \\ k_{\mathrm{iL}} = & 1.6325\times10^{9}\rho^{0.55}\cdot\exp\left(\dfrac{-44.78T_0}{T}\right) \\ \mu_{\mathrm{i}} = & 0.008626\rho^5+0.063737\rho^4-0.2628\rho^3 \\ & -1.18668\rho^2-2.9749\rho+30.0 \\ \xi_{\mathrm{ci}} = & 0.00018\rho^3+0.000359\rho^2 \\ & -0.081826\rho+0.828095 \end{cases}$$

A.2.6 Lean acetylene–oxygen mixture ($\phi = 0.5$)

Reactants: $2C_2H_2 + 10O_2$
Mechanism: Konnov [35]
Equilibrium relation coefficients:

$$\begin{cases} \alpha_1 = 25.2274 & \alpha_2 = -1.718726 \\ \beta_0 = 3.335907 & \beta_1 = -0.711998 \\ \beta_2 = 0.5399 & \delta_0 = 12.19536 \\ \delta_1 = 0.20035 & \delta_2 = 0.0053149 \end{cases}$$

Reaction orders:

$$\begin{cases} s_0 = 0.339 & s_1 = 0.85 \\ s_2 = 0.85 & s_3 = 1.02 \end{cases}$$

$$k_{\mathrm{ef}} = 5.66\times10^{29}\rho^{1.022}T^{-4.655}\cdot\exp\left(\frac{-231.1T_0}{T}\right)$$

$$k_{\mathrm{r1}}\begin{cases} k_{\mathrm{r1H}} = 5.787\times10^{9}\rho^{1.038}\cdot\exp\left(\dfrac{-47.51T_0}{T}\right) \\ k_{\mathrm{r1L}} = 1.307\times10^{9}\rho^{1.109}\cdot\exp\left(\dfrac{-38.46T_0}{T}\right) \\ \mu_{\mathrm{r1}} = 42.8557; \quad \xi_{\mathrm{c1}} = 0.19826+\dfrac{0.06223}{\rho^{0.1}} \end{cases}$$

$$k_{\mathrm{r2}}\begin{cases} k_{\mathrm{r2H}} = 3.091\times10^{9}\rho^{1.027}\cdot\exp\left(\dfrac{-54.55T_0}{T}\right) \\ k_{\mathrm{r2L}} = 5.843\times10^{8}\rho^{1.115}\cdot\exp\left(\dfrac{-43.82T_0}{T}\right) \\ \mu_{\mathrm{r2}} = 48.46338; \quad \xi_{\mathrm{c2}} = 0.1989+\dfrac{0.071355}{\rho^{0.1}} \end{cases}$$

$$k_{\mathrm{i}}\begin{cases} k_{\mathrm{iH}} = & 4.05\times10^{-3}\rho^{0.70441}T^{3.05118} \\ & \cdot\exp\left(\dfrac{-11.4966T_0}{T}\right) \\ k_{\mathrm{iL}} = & 9.91749\times10^{8}\rho^{0.63}\cdot\exp\left(\dfrac{-45.77T_0}{T}\right) \\ \mu_{\mathrm{i}} = & 0.002832\rho^5+0.01038\rho^4-0.0546\rho^3 \\ & +0.4165\rho^2-3.0473\rho+20.0 \\ \xi_{\mathrm{ci}} = & 0.0002655\rho^3+0.0010179\rho^2 \\ & -0.0753064\rho+0.80079 \end{cases}$$

A.2.7 Lean acetylene–oxygen mixture ($\phi = 0.33$)

Reactants: $2C_2H_2 + 15O_2$
Mechanism: Konnov [35]
Equilibrium relation coefficients:

$$\begin{cases} \alpha_1 = 24.650396 & \alpha_2 = -1.721397 \\ \beta_0 = 3.357345 & \beta_1 = -0.771712 \\ \beta_2 = 0.47847 & \delta_0 = 11.789399 \\ \delta_1 = 0.167798 & \delta_2 = 0.0049935 \end{cases}$$

Reaction orders:

$$\begin{cases} s_0 = 0.339 & s_1 = 0.867 \\ s_2 = 0.867 & s_3 = 1.09 \end{cases}$$

$$k_{\mathrm{ef}} = 1.276\times10^{24}\rho^{0.9248}T^{-3.304}\cdot\exp\left(\frac{-213.9T_0}{T}\right)$$

$$k_{\mathrm{r1}}\begin{cases} k_{\mathrm{r1H}} = 6.575\times10^{9}\rho^{1.002}\cdot\exp\left(\dfrac{-49.35T_0}{T}\right) \\ k_{\mathrm{r1L}} = 1.709\times10^{9}\rho^{1.097}\cdot\exp\left(\dfrac{-38.72T_0}{T}\right) \\ \mu_{\mathrm{r1}} = 15.692; \quad \xi_{\mathrm{c1}} = 0.271+\dfrac{0.0009}{\rho^{0.8415}} \end{cases}$$

$$k_{\mathrm{r2}}\begin{cases} k_{\mathrm{r2H}} = 3.587\times10^{9}\rho^{0.9857}\cdot\exp\left(\dfrac{-63.19T_0}{T}\right) \\ k_{\mathrm{r2L}} = 4.885\times10^{8}\rho^{1.092}\cdot\exp\left(\dfrac{-43.85T_0}{T}\right) \\ \mu_{\mathrm{r2}} = 24.9728; \quad \xi_{\mathrm{c2}} = 0.25947+\dfrac{0.099}{\rho^{0.1}} \end{cases}$$

$$k_{\mathrm{i}}\begin{cases} k_{\mathrm{iH}} = & 2.122\times10^{-2}\rho^{0.628}T^{2.865} \\ & \cdot\exp\left(\dfrac{-16.817T_0}{T}\right) \\ k_{\mathrm{iL}} = & 7.13138\times10^{8}\rho^{0.61077} \\ & \cdot\exp\left(\dfrac{-45.973T_0}{T}\right) \\ \mu_{\mathrm{i}} = & 0.00515\rho^5+0.023716\rho^4-0.15017\rho^3 \\ & -0.031435\rho^2-3.4744\rho+25.0 \\ \xi_{\mathrm{ci}} = & 0.0005\rho^3+0.00226\rho^2 \\ & -0.08338\rho+0.83397 \end{cases}$$

Acknowledgements BM would like to acknowledge correspondence with J. Yang and Y. Zhu for helpful advice toward understanding and developing the four-step model parameters used in this paper.

Funding The authors did not receive support from any organization for the submitted work.

Availability of data and materials The datasets generated during and/or analyzed during the current study are available from the corresponding author on reasonable request.

Declarations

Conflict of interest The authors have no competing interests to declare that are relevant to the content of this article.

References

1. Oran, E.S., Gamezo, V.N.: Origins of the deflagration-to-detonation transition in gas-phase combustion. Combust. Flame **148**, 4–47 (2007). https://doi.org/10.1016/j.combustflame.2006.07.010
2. Mazaheri, K.: Mechanism of the onset of detonation in direct initiation. PhD thesis, Department of Mechanical Engineering, McGill University, Canada (1997). https://escholarship.mcgill.ca/concern/theses/qv33rz410
3. Short, M., Kapila, A.K., Quirk, J.J.: The chemical-gas dynamic mechanisms of pulsating detonation wave instability. Philos. Trans. R. Soc. A **357**, 3621–3637 (1999). https://doi.org/10.1098/rsta.1999.0513
4. Liberman, M., Wang, C., Qian, C., Liu, J.: Influence of chemical kinetics on spontaneous waves and detonation initiation in highly reactive and low reactive mixtures. Combust. Theor. Model. **23**, 467–495 (2019). https://doi.org/10.1080/13647830.2018.1551578
5. Dounia, O., Vermorel, O., Misdariis, A., Poinsot, T.: Influence of kinetics on DDT simulations. Combust. Flame **200**, 1–14 (2019). https://doi.org/10.1016/j.combustflame.2018.11.009

6. Turányi, T.: Applications of sensitivity analysis to combustion chemistry. Reliab. Eng. Syst. Safe **57**, 41–48 (1997). https://doi.org/10.1016/S0951-8320(97)00016-1
7. Massias, A., Diamantis, D., Mastorakos, E., Goussis, D.: An algorithm for the construction of global reduced mechanisms with CSP data. Combust. Flame **117**, 685–708 (1999). https://doi.org/10.1016/S0010-2180(98)00132-1
8. Lu, T., Ju, Y., Law, C.K.: Complex CSP for chemistry reduction and analysis. Combust. Flame **126**, 1445–1455 (2001). https://doi.org/10.1016/S0010-2180(01)00252-8
9. Bhattacharjee, B., Schwer, D.A., Barton, P.I., Green, W.H.: Optimally-reduced kinetic models: reaction elimination in large-scale kinetic mechanisms. Combust. Flame **135**, 191–208 (2003). https://doi.org/10.1016/S0010-2180(03)00159-7
10. Varatharajan, B., Williams, F.: Chemical-kinetic descriptions of high-temperature ignition and detonation of acetylene-oxygen-diluent systems. Combust. Flame **124**, 624–645 (2001). https://doi.org/10.1016/S0010-2180(00)00235-2
11. Lam, S., Goussis, D.: The CSP method for simplifying kinetics. Int. J. Chem. Kinet. **26**, 461–486 (1994). https://doi.org/10.1002/kin.550260408
12. Maas, U., Pope, S.B.: Simplifying chemical kinetics: intrinsic low-dimensional manifolds in composition space. Combust. Flame **88**, 239–264 (1992). https://doi.org/10.1016/0010-2180(92)90034-M
13. Lu, T., Law, C.K.: Toward accommodating realistic fuel chemistry in large-scale computations. Prog. Energy Combust. **35**, 192–215 (2009). https://doi.org/10.1016/j.pecs.2008.10.002
14. Lu, T., Law, C.K.: A directed relation graph method for mechanism reduction. Proc. Combust. Inst. **30**, 1333–1341 (2005). https://doi.org/10.1016/j.proci.2004.08.145
15. Zambon, A.C., Chelliah, H.K.: Explicit reduced reaction models for ignition, flame propagation, and extinction of $C_2H_4/CH_4/H_2$ and air systems. Combust. Flame **150**, 71–91 (2007). https://doi.org/10.1016/j.combustflame.2007.03.003
16. Williams, F.A.: Combustion Theory. CRC Press, Boca Raton (2018)
17. Arienti, M., Shepherd, J.E.: A numerical study of detonation diffraction. J. Fluid Mech. **529**, 117–146 (2005). https://doi.org/10.1017/S0022112005003319
18. Leung, C., Radulescu, M.I., Sharpe, G.J.: Characteristics analysis of the one-dimensional pulsating dynamics of chain-branching detonations. Phys. Fluids **22**, 126101 (2010). https://doi.org/10.1063/1.3520188
19. Radulescu, M., Sharpe, G., Bradley, D.: A universal parameter quantifying explosion hazards, detonability and hot spot formation: the χ number. ISFEH7 Proceedings of the Seventh International Seminar (2013)
20. Ng, H., Radulescu, M., Higgins, A., Nikiforakis, N., Lee, J.: Numerical investigation of the instability for one-dimensional Chapman Jouguet detonations with chain-branching kinetics. Combust. Theor. Model. **9**, 385–401 (2005). https://doi.org/10.1080/13647830500307758
21. Dold, J.W., Kapila, A.K.: Comparison between shock initiations of detonation using thermally-sensitive and chain-branching chemical models. Combust. Flame **85**, 185–194 (1991). https://doi.org/10.1016/0010-2180(91)90186-F
22. Short, M., Quirk, J.J.: On the nonlinear stability and detonability limit of a detonation wave for a model three-step chain-branching reaction. J. Fluid Mech. **339**, 89–119 (1997). https://doi.org/10.1017/S002211209700503X
23. Mazaheri, K., Hashemi, S.A.: The effect of chain initiation reaction on the stability of gaseous detonations. Combust. Sci. Technol. **179**, 1701–1736 (2007). https://doi.org/10.1080/00102200701259916
24. Blythe, P., Kapila, A.K., Short, M.: Homogeneous ignition for a three-step chain-branching reaction model. J. Eng. Math. **60**, 125–126 (2006). https://doi.org/10.1007/s10665-006-9055-0
25. Ng, H.D., Lee, J.H.S.: Direct initiation of detonation with a multi-step reaction scheme. J. Fluid Mech. **476**, 179–211 (2003). https://doi.org/10.1017/S0022112002002872
26. Liang, Z., Bauwens, L.: Cell structure and stability of detonations with a pressure-dependent chain-branching reaction rate model. Combust. Theor. Model. **9**, 93–112 (2005). https://doi.org/10.1080/13647830500051885
27. Liang, Z., Browne, S., Deiterding, R., Shepherd, J.: Detonation front structure and the competition for radicals. Proc. Combust. Inst. **31**, 2445–2453 (2007). https://doi.org/10.1016/j.proci.2006.07.244
28. Urtiew, P.A., Oppenheim, A.K.: Experimental observations of the transition to detonation in an explosive gas. Proc. R. Soc. Lond. A Math. **295**, 13–28 (1966). https://doi.org/10.1098/rspa.1966.0223
29. Ciccarelli, G., Dorofeev, S.: Flame acceleration and transition to detonation in ducts. Prog. Energy Combust. **34**, 499–550 (2008). https://doi.org/10.1016/j.pecs.2007.11.002
30. Thomas, G., Bambrey, R., Brown, C.: Experimental observations of flame acceleration and transition to detonation following shock-flame interaction. Combust. Theor. Model. **5**, 573–594 (2001). https://doi.org/10.1088/1364-7830/5/4/304
31. Zhu, Y., Yang, J., Sun, M.: A thermochemically derived global reaction mechanism for detonation application. Shock Waves **22**, 363–379 (2012). https://doi.org/10.1007/s00193-012-0375-x
32. Goodwin, D.G., Speth, R.L., Moffat, H.K., Weber, B.W.: Cantera: An Object-oriented Software Toolkit for Chemical Kinetics, Thermodynamics, and Transport Processes. https://www.cantera.org. Version 2.4.0 (2018)
33. Fickett, W., Jacobson, J.D., Schott, G.L.: Calculated pulsating one-dimensional detonations with induction-zone kinetics. AIAA J. **10**, 514–516 (1972). https://doi.org/10.2514/3.50130
34. Clarke, J.F.: The pre-mixed flame with large activation energy and variable mixture strength: elementary asymptotic analysis. Combust. Sci. Technol. **10**, 189–194 (1975). https://doi.org/10.1080/00102207508946670
35. Coppens, F.H.V., De Ruyck, J., Konnov, A.A.: The effects of composition on burning velocity and nitric oxide formation in laminar premixed flames of $CH_4 + H_2 + O_2 + N_2$. Combust. Flame **149**, 409–417 (2007). https://doi.org/10.1016/j.combustflame.2007.02.004
36. Smith, G.P., Golden, D.M., Frenklach, M., Moriarty, N.W., Eiteneer, B., Goldenberg, M., Bowman, C.T., Hanson, R.K., Song, S., Gardiner Jr, W.C., Lissianski, V.V., Qin, Z.: GRI 3.0 Mechanism (1999). http://www.me.berkeley.edu/gri_mech/
37. Wang, H., You, X., Joshi, A.V., Davis, S.G., Laskin, A., Egolfopoulos, F., Law, C.: USC Mech Version II. High-temperature combustion reaction model of H_2/CO/C1-C4 compounds. http://ignis.usc.edu/USC_Mech_II.htm. Combustion Kinetics Laboratory, University of Southern California, Los Angeles, CA (2007)
38. Fickett, W., Davis, W.C.: Detonation: Theory and Experiment. Dover Publications, Mineola (2000)
39. Kao, S., Shepherd, J.: Numerical solution methods for control volume explosions and ZND detonation structure. GALCIT Report FM2006 **7**, 1–46 (2008)
40. McBride, B.J.: Coefficients for Calculating Thermodynamic and Transport Properties of Individual Species. NASA Langley Research Center, Hampton (1993)
41. Hindmarsh, A.C., Brown, P.N., Grant, K.E., Lee, S.L., Serban, R., Shumaker, D.E., Woodward, C.S.: SUNDIALS: suite of nonlinear and differential/algebraic equation solvers. ACM Trans. Math. Softw. **31**, 363–396 (2005). https://doi.org/10.1145/1089014.1089020
42. Peswani, M., Maxwell, B.M.: Performance of a generic 4-step global reaction mechanism with equilibrium effects for detonation applications. ASME Int. Mech. Eng. Congress Expo. (2020). https://doi.org/10.1115/IMECE2020-23786

43. Maxwell, B., Pekalski, A., Radulescu, M.: Modelling of the transition of a turbulent shock-flame complex to detonation using the linear eddy model. Combust. Flame **192**, 340–357 (2018). https://doi.org/10.1016/j.combustflame.2018.02.013
44. Maxwell, B.M., Bhattacharjee, R.R., Lau-Chapdelaine, S.S.M., Falle, S.A.E.G., Sharpe, G.J., Radulescu, M.I.: Influence of turbulent fluctuations on detonation propagation. J. Fluid Mech. **818**, 646–696 (2017). https://doi.org/10.1017/jfm.2017.145
45. Browne, S., Ziegler, J., Shepherd, J.: Numerical solution methods for shock and detonation jump conditions. GALCIT Report FM2006 **6**, 90 (2008)
46. Radulescu, M.I., Ng, H.D., Lee, J.H.S., Varatharajan, B.: The effect of argon dilution on the stability of acetylene/oxygen detonations. Proc. Combust. Inst. **29**, 2825–2831 (2002). https://doi.org/10.1016/S1540-7489(02)80345-5
47. Dayma, G., Halter, F., Dagaut, P.: New insights into the peculiar behavior of laminar burning velocities of hydrogen-air flames according to pressure and equivalence ratio. Combust. Flame **161**, 2235–2241 (2014). https://doi.org/10.1016/j.combustflame.2014.02.009
48. Kamal, M.M., Barlow, R.S., Hochgreb, S.: Conditional analysis of turbulent premixed and stratified flames on local equivalence ratio and progress of reaction. Combust. Flame **162**, 3896–3913 (2015). https://doi.org/10.1016/j.combustflame.2015.07.026
49. Hasson, A., Avinor, M., Burcat, A.: Transition from deflagration to detonation, spark ignition, and detonation characteristics of ethylene-oxygen mixtures in a tube. Combust. Flame **49**, 13–26 (1983). https://doi.org/10.1016/0010-2180(83)90147-5
50. Dorofeev, S.B.: Hydrogen flames in tubes: critical run-up distances. Int. J. Hydrogen Energy **34**, 5832–5837 (2009). https://doi.org/10.1016/j.ijhydene.2009.01.008
51. Tang, J., Radulescu, M.I.: Dynamics of shock induced ignition in Fickett's model: influence of χ. Proc. Combust. Inst. **34**, 2035–2041 (2013). https://doi.org/10.1016/j.proci.2012.05.079
52. Wang, Xç., Law, C.K.: An analysis of the explosion limits of hydrogen-oxygen mixtures. J. Chem. Phys. **138**(13), 134305 (2013). https://doi.org/10.1063/1.4798459
53. Townend, D.T., Chamberlain, E.: The influence of pressure on the spontaneous ignition and limits of inflammability of ether-air mixtures. Proc. R. Soc. Lond. Ser. A Math. Phys. Sci. **158**(894), 415–429 (1937)
54. Newitt, D.M., Thornes, L.S.: 348. The oxidation of propane. Part I, the products of the slow oxidation at atmospheric and at reduced pressures. J. Chem. Soc. (1937). https://doi.org/10.1039/JR9370001656
55. Liu, J., Yu, R., Ma, B., Tang, C.: On the second explosion limits of hydrogen, methane, ethane, and propane. ACS Omega **5**(30), 19268–19276 (2020). https://doi.org/10.1021/acsomega.0c02825. (**PMID: 32775930**)
56. Li, Y., Zhou, C.-W., Somers, K.P., Zhang, K., Curran, H.J.: The oxidation of 2-butene: a high pressure ignition delay, kinetic modeling study and reactivity comparison with isobutene and 1-butene. Proc. Combust. Inst. **36**(1), 403–411 (2017). https://doi.org/10.1016/j.proci.2016.05.052
57. Burgess, D.: Combustion, flames, and explosions of gases. J. Chem. Educ. **39**(4), 312 (1962). https://doi.org/10.1021/ed039pA312.2
58. Austin, J.M.: The role of instability in gaseous detonation. PhD thesis, California Institute of Technology Pasadena (2003). https://resolver.caltech.edu/CaltechETD:etd-05292003-150534
59. Shepherd, J.: Shock & detonation toolbox-Cantera 2.1. Explosion Dynamics Laboratory, California Institute of Technology. Accessed 11 Oct 2019 (2018)
60. Borzou, B., Maxwell, B., Radulescu, M.I.: Influence of the reaction-to-induction length ratio on the stability of cellular detonations. 23rd International Colloquium on the Dynamics of Explosions and Reactive Systems, Irvine, USA (2011)
61. Short, M., Sharpe, G.J.: Pulsating instability of detonations with a two-step chain-branching reaction model: theory and numerics. Combust. Theor. Model. **7**, 401–416 (2003). https://doi.org/10.1088/1364-7830/7/2/311
62. Ng, H.D., Radulescu, M.I., Higgins, A.J., Nikiforakis, N., Lee, J.H.S.: Numerical investigation of the instability for one-dimensional Chapman–Jouguet detonations with chain-branching kinetics. Combust. Theor. Model. **9**, 385–401 (2005). https://doi.org/10.1080/13647830500307758
63. Maxwell, B.M.: Turbulent combustion modelling of fast-flames and detonations using compressible LEM-LES. PhD thesis, Université d'Ottawa/University of Ottawa (2016). http://dx.doi.org/10.20381/ruor-5339
64. Borzou, B., Radulescu, M.I.: Evaluation of hydrogen, propane and methane-air detonations instability and detonability. International Conference on Hydrogen Safety, ICHS, Brussels, Belgium (2013)
65. Taileb, S., Melguizo-Gavilanes, J., Chinnayya, A.: Influence of the chemical modeling on the quenching limits of gaseous detonation waves confined by an inert layer. Combust. Flame **218**, 247–259 (2020). https://doi.org/10.1016/j.combustflame.2020.04.018
66. Radulescu, M.I.: The propagation and failure mechanism of gaseous detonations: experiments in porous-walled tubes. PhD thesis, McGill University Libraries (2003). https://escholarship.mcgill.ca/concern/theses/w37637360
67. Zeldovich, J.B., Frank-Kamenetzki, D.A.: A theory of thermal propagation of flame. In: Pelcé, P. (ed.) Dynamics of Curved Fronts, pp. 131–140. Academic Press (1988). https://doi.org/10.1016/B978-0-08-092523-3.50015-0
68. Zeldovich, I., Barenblatt, G.I., Librovich, V., Makhviladze, G.: Mathematical Theory of Combustion and Explosions. Consultants Bureau, New York (1985)
69. Peraldi, O., Knystautas, R., Lee, J.H.: Criteria for transition to detonation in tubes. Proc. Combust. Inst. **21**, 1629–1637 (1988). https://doi.org/10.1016/S0082-0784(88)80396-5
70. Dorofeev, S.B., Kuznetsov, M.S., Alekseev, V.I., Efimenko, A.A., Breitung, W.: Evaluation of limits for effective flame acceleration in hydrogen mixtures. J. Loss Prev. Process **14**, 583–589 (2001). https://doi.org/10.1016/S0950-4230(01)00050-X
71. Schultz, E., Wintenberger, E., Shepherd, J.: Investigation of deflagration to detonation transition for application to pulse detonation engine ignition systems. 36th JANNAF Combustion and Airbreathing Propulsion Subcommittees Meeting, Cocoa Beach (1999)
72. Bane, S., Ziegler, J., Shepherd, J.: Development of one-step chemistry models for flame and ignition simulation. GALCIT Rep. **2**, 53 (2010)
73. Hu, F., Li, P., Wang, K., Li, W., Guo, J., Liu, L., Liu, Z.: Evaluation, development, and application of a new skeletal mechanism for fuel-no formation under air and oxy-fuel combustion. Fuel Process. Technol. **199**, 106256 (2020). https://doi.org/10.1016/j.fuproc.2019.106256
74. Olm, C., Zsély, I.G., Pálvölgyi, R., Varga, T., Nagy, T., Curran, H.J., Turányi, T.: Comparison of the performance of several recent hydrogen combustion mechanisms. Combust. Flame **161**(9), 2219–2234 (2014). https://doi.org/10.1016/j.combustflame.2014.03.006

75. Alturaifi, S.A., Mulvihill, C.R., Mathieu, O., Petersen, E.L.: Speciation measurements in shock tubes for validation of complex chemical kinetics mechanisms: application to 2-methyl-2-butene oxidation. Combust. Flame **225**, 196–213 (2021). https://doi.org/10.1016/j.combustflame.2020.10.041